

 **π -Conjugated Polymers and Molecules Enabling Small Photon Energy Loss in Organic Photovoltaics**

Journal:	<i>Journal of Materials Chemistry A</i>
Manuscript ID	TA-REV-05-2020-005108.R1
Article Type:	Review Article
Date Submitted by the Author:	29-Jul-2020
Complete List of Authors:	Osaka, Itaru; Hiroshima Daigaku, Applied Chemistry Saito, Masahiko; Hiroshima University, Department of Applied Chemistry Ohkita, Hideo; Kyoto University, Department of Polymer Chemistry

SCHOLARONE™
Manuscripts

π -Conjugated Polymers and Molecules Enabling Small Photon Energy Loss Simultaneously with High Efficiency in Organic Photovoltaics

Masahiko Saito^{1,2}, Hideo Ohkita^{3*}, and Itaru Osaka^{1,2*}

¹ *Department of Applied Chemistry, Graduate School of Engineering, Hiroshima University, 1-4-1 Kagamiyama, Higashi-Hiroshima, Hiroshima 739-8527, Japan*

² *Department of Applied Chemistry, Graduate School of Advanced Science and Engineering, Hiroshima University, 1-4-1 Kagamiyama, Higashi-Hiroshima, Hiroshima 739-8527, Japan*

³ *Department of Polymer Chemistry, Graduate School of Engineering, Kyoto University, Katsura, Nishikyo-ku, Kyoto 615-8510, Japan*

E-mail address: ohkita@photo.polym.kyoto-u.ac.jp, iosaka@hiroshima-u.ac.jp

Abstract

Organic photovoltaics (OPVs) are a topic of significant research interest in the field of renewable energy as well as organic electronics. The crucial issue in OPVs is the improvement of the power conversion efficiency (PCE). In addressing this issue, one of the most important factors is the photon energy loss (E_{loss}), which is defined as the difference between the bandgap of the materials and the energy corresponding to the open-circuit voltage. Typically, the E_{loss} for OPVs is considerably larger than that for inorganic and perovskite photovoltaics, which has prevented OPVs from generating larger photovoltages. In parallel, reducing the E_{loss} for OPVs causes a loss of driving-force energy for charge generation, which is detrimental to the generation of photocurrent. Thus, OPVs have been facing a trade-off between photocurrent and photovoltage. However, a number of recently developed π -conjugated materials for use as p-type and n-type organic semiconductors have shown to enable small E_{loss} values that are close to those for inorganic systems, simultaneously with efficient charge generation. Here, we summarize recent progress in π -conjugated polymers and molecules that enable small E_{loss} and high PCE at the same time. We hope that this review will be of help to chemists and materials scientists who are involved in the design of materials and blends with an eye toward highly efficient OPVs.

1. Introduction

Organic photovoltaics (OPVs) are a topic of significant research interest in the field of renewable energy owing to their solution processability, lightweight nature, and flexibility.^{1,2} The photoactive layer of the OPV cell is composed of p-type and n-type organic semiconductors (electron donor and acceptor materials, respectively) that are blended together to form a bulk heterojunction film.^{1,3,4,5,6} Typically, π -conjugated polymers are employed as the p-type semiconductor in combination with π -conjugated molecules, such as fullerene⁷ and non-fullerene derivatives,⁸ or π -conjugated polymers⁹ as the n-type semiconductor. Owing to the considerable effort in the development of those organic semiconductors,^{10,11,12,13,14,15,16,17,18,19} the power conversion efficiencies (PCEs) for OPVs have made significant advances to more than 17%:^{20,21,22,23} the long-standing milestone of 10% PCE is no longer a rarity.

The PCEs for OPVs, however, remain low relative to those for silicon ($\sim 25\%$)^{24,25} and perovskite ($\sim 25\%$)^{21,26} photovoltaics (PVs). The foremost reason for this is the significant loss of the voltage, originating in the loss of energy during the photoconversion process, which is called photon energy loss (E_{loss}) or simply energy loss. The E_{loss} is defined as the difference between the bandgap (E_{g}) of the material and the energy corresponding to the open-circuit voltage (V_{OC}) for the photovoltaic cell, $E_{\text{loss}} = E_{\text{g}} - qV_{\text{OC}}$ (or eV_{OC}), where both q and e are elementary charge,^{27,28} i.e., the difference between the incident photon (input) energy and the output energy. Note that the E_{loss} can also be expressed as the voltage loss (V_{loss}): $V_{\text{loss}} = E_{\text{g}}/q - V_{\text{OC}}$. The E_{loss} for high-efficiency OPVs, specifically polymer/fullerene systems, had been typically more than 0.7 eV.^{27,29,30} This is considerably larger than those for silicon (~ 0.4 eV)^{24,28} and perovskite (~ 0.4 eV)^{21,31} PVs. Thus, the large E_{loss} had been a critical disadvantage in producing a high V_{OC} and a fundamental issue that must be resolved for further PCE improvement in OPVs. Fortunately, however, recent efforts in the development of new organic semiconductor materials and optimization of their blends have brought about remarkable reduction of the E_{loss} down to ~ 0.5 eV (**Figure 1a**), which is much smaller than the value of 0.6 eV that was suggested as the minimum E_{loss} for OPV to exhibit a certain level of performance.²⁷

Moreover, although there has been a trade-off between the E_{loss} and the external quantum efficiency (EQE), where the EQE significantly decreases when the E_{loss} is decreased³² as will be described in depth below, the state-of-the-art OPV devices can now give high EQEs of around 80% at E_{loss} s of around 0.5 eV, consequently resulting in high PCEs of >17% (**Figures 1b and c**).

In this review, we first describe the origin of E_{loss} and the issues for the E_{loss} reduction, and then summarize organic semiconductor systems that enable small E_{loss} for OPVs. We discuss the topic by classifying into polymer/fullerene and polymer/non-fullerene systems. In the polymer/fullerene section, fullerene derivatives and narrow-bandgap p-type π -conjugated polymers are described, and in the polymer/non-fullerene section, wide-bandgap n-type π -conjugated molecules, narrow-bandgap π -conjugated molecules along with wide-bandgap p-type π -conjugated polymers that match these non-fullerene systems, and n-type π -conjugated polymers are presented. Although the current benchmark for “small E_{loss} ” for OPVs would probably be 0.6 eV, we do not limit the materials systems discussed herein to this value. Rather, we focus on how the research on this topic has advanced from the perspective of materials development and discuss what materials and blends tend to have small E_{loss} s simultaneously with high PCEs. We hope that this review will be of help to chemists and materials scientists in this area in the further design of high-performance π -conjugated materials for OPVs.

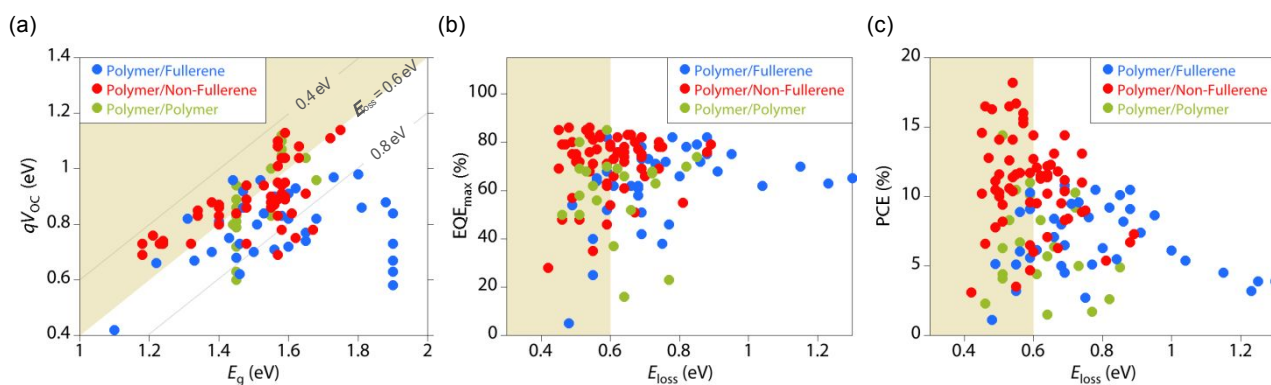


Figure 1. (a) Plots of qV_{OC} versus E_g , and (b) plots of maximum external quantum efficiency (EQE_{max}) versus E_{loss} ($E_g - qV_{OC}$), (c) plots of power conversion efficiency versus E_{loss} ($E_g - qV_{OC}$) for polymer/fullerene (blue dots), polymer/non-fullerene (red dots), and polymer/polymer cells (green dots).

2. Origin of photon energy loss (E_{loss}) and issues for E_{loss} reduction

The origin of the large E_{loss} for OPVs can be understood by considering the working principle. **Figure 2a** shows the energy level diagrams of pairs of p-type and n-type organic semiconductors.³³ It is widely accepted that the OPV cell undergoes efficient charge generation only when there is a certain amount of offset in the energy level of the lowest unoccupied molecular orbitals (LUMOs) (**Figure 2a**, left) or the highest occupied molecular orbitals (HOMOs) (**Figure 2a**, right) between the p-type and n-type organic semiconductors (ΔE_L or ΔE_H). Note that one would consider the offset energy as ΔE_L or ΔE_H when the p-type or n-type organic semiconductor is the narrower bandgap material, respectively. The offset energy is thought to be the driving-force energy to overcome the binding energy of an electron–hole pair in the excitons generated by photoexcitation of the p-type and/or n-type organic semiconductors, respectively, and are reported to be typically more than 0.3 eV.^{34,35,36} In parallel, the offset energy will be lost in the charge generation process, thereby accounting for one of the factors for the E_{loss} . In sharp contrast, as inorganic and perovskite photovoltaics directly generate free charge carriers immediately after the photon absorption because

excitons can be spontaneously dissociated into free charge carriers even at room temperature owing to the large dielectric constants, they do not require such driving-force energy for charge generation.³⁷ Thus, it is clear that the offset energy is an additional factor for the E_{loss} that is unique to OPVs. As a result, whereas the V_{OC} for inorganic and perovskite systems is determined on the basis of the E_{g} of the semiconductor material, the V_{OC} for OPVs is determined on the basis of the energy between the HOMO of the p-type and the LUMO of the n-type (ΔE_{HL}), which is considered as the effective bandgap of the blend and is smaller than the E_{g} of both organic semiconductors, leading to lower V_{OC} s.

The E_{loss} can also be described by using a state energy diagram (**Figures 2b** and **2c**). E_{loss} can mainly be classified into two categories, which are two recombination losses originating in radiative and non-radiative recombinations ($q\Delta V_{\text{r}}$ and $q\Delta V_{\text{nr}}$). Note that whereas in the Shockley–Queisser (SQ) theory,³⁸⁻⁴⁰ E_{loss} is assumed to be only due to $q\Delta V_{\text{r}}$, which can be calculated by using a step-function absorption where absorptance is zero below E_{g} and unity above E_{g} , in the real PV devices, E_{loss} consists of both $q\Delta V_{\text{r}}$ and $q\Delta V_{\text{nr}}$. It is also noted that there is an additional energy loss factor due to the decrease in the short-circuit current (J_{SC}), which is often ignored since this is generally negligibly small (see the Supplementary Information) and thus is not described in this paper as well. **Figure 2b** shows the relationship among the input energy (E_{g}), output voltage energy (qV_{OC}), and loss energy (E_{loss}) for inorganic and perovskite PVs, in which E_{loss} is mainly due to $q\Delta V_{\text{r}}$ and $q\Delta V_{\text{nr}}$ ($E_{\text{loss}} = q\Delta V_{\text{r}} + q\Delta V_{\text{nr}}$). In addition, $q\Delta V_{\text{r}}$ is further classified into losses above and below E_{g} ($q\Delta V_{\text{r1}}$ and $q\Delta V_{\text{r2}}$) because of additional absorption below E_{g} .³⁸⁻⁴⁰ On the other hand, the relationship among E_{g} , qV_{OC} , and E_{loss} for OPVs can be illustrated as shown in **Figure 2c**. A striking difference from the inorganic systems is that the charge transfer (CT) state, being formed at the p/n interface,^{41, 42} must be taken into consideration for E_{loss} .²² The energy of the CT state (E_{CT}) is lower than that of the singlet exciton or singlet excited (S_1) state (E_{S1}) of the system, so that the excitons can be efficiently converted into free charge carriers. Therefore, E_{loss} can be expressed as $E_{\text{loss}} = \Delta E + q\Delta V_{\text{r,CT}} + q\Delta V_{\text{nr}}$, where ΔE is the energy difference between E_{S1} and E_{CT} , thus being regarded as the loss due to charge

transfer, and $q\Delta V_{r,CT}$ is the loss due to the radiative recombination.⁴³ Note that as the E_{S1} and E_{CT} are qualitatively equal to the narrower E_g of the two organic semiconductors and the ΔE_{HL} , respectively,⁴⁴ ΔE is qualitatively equal to ΔE_L or ΔE_H , i.e., the driving-force energy for charge generation. Consequently, the E_{loss} for OPV is larger than that for inorganic and perovskite PVs due to ΔE being lost at the CT process. We should also note that radiative recombination losses $q\Delta V_r$ and $q\Delta V_{r,CT}$ shown in **Figures 2b** and **2c**, respectively, is different. The $q\Delta V_r$ is the radiative loss based on E_g , which is dependent only on E_g , while the $q\Delta V_{r,CT}$ is radiative loss based on E_{CT} , which is dependent not only on E_{CT} but also on ΔE : $q\Delta V_{r,CT}$ decreases with the increase in ΔE (see the Supplementary Information). In addition, as shown in **Figure 2c**, the E_{loss} in OPVs can also be explained without using ΔE in the same way as in inorganic and perovskite PVs, where the radiative loss is considered as the loss based on E_g , thus shown as $q\Delta V_r$, and is classified into the loss above and below E_g ($q\Delta V_{r1}$ and $q\Delta V_{r2}$). In this case, the CT absorption is considered as an additional absorption below E_g , which is typically much larger than that of the absorption tail for inorganic and perovskite PVs. Thus, $q\Delta V_{r2}$ is larger in OPVs than in inorganic and perovskite solar cells while $q\Delta V_{r1}$ is similar, resulting in larger radiative loss and in turn E_{loss} .

Given the mechanism and the loss factors of OPVs discussed above, it is clear that reducing the offset energy, ΔE_L or $\Delta E_H \approx \Delta E$, by tuning the energy level of the materials is essential to minimize the E_{loss} for OPVs. However, reduction of the offset energy implies loss of the driving-force energy for charge generation, which gives rise to low EQEs and thus to low J_{SC} s, which are rather detrimental to the PCE improvement, although results in high V_{OC} s. Thus, there is a clear trade-off between E_{loss} and efficient charge generation, or more simply, between V_{OC} and J_{SC} . In fact, when data from a range of polymer/fullerene systems were collected, the EQE as well as PCE was found to decrease with the decrease in the E_{loss} (**Figure 1b** and **1c**, blue dots). Note that, however, recent studies have shown that even with the E_{loss} of less than 0.6 eV that had been suggested for the minimum value, some particular polymer/fullerene systems can undergo efficient charge generation, resulting in relatively high EQEs of >60%.^{29,30,32} More recently, the use of non-fullerenes as the n-type organic

semiconductors was found to provide even higher EQEs of reaching 80% with similarly small E_{loss} s (**Figure 1b**, red dots).^{45, 46} In addition, some polymer/polymer (all-polymer) cells were also reported to show high EQEs of ~80% with E_{loss} s of less than 0.6 eV, though the number is limited (**Figure 1b**, green dots).

With respect to the loss factor due to the non-radiative recombination, $q\Delta V_{\text{nr}}$, it is expressed as $-k_{\text{B}}T \ln(\text{EQE}_{\text{EL}})$, where k_{B} is the Boltzmann constant, T is the temperature, and EQE_{EL} is EQE of electroluminescence (EL) of the photovoltaic cell. Thus, a photovoltaic cell as a good light-emitting diode shows small $q\Delta V_{\text{nr}}$.^{47, 48} In general, OPV cells show $q\Delta V_{\text{nr}}$ of ~0.4 eV, which is larger than ~0.2 eV for silicon and perovskite photovoltaics, originating in the fact that the active layer is composed of a heterojunction of two different materials and thus CT emission is dominant. However, it is reported that the blend systems with a small ΔE show relatively high EQE_{EL} and thus small $q\Delta V_{\text{nr}}$ values below 0.3 eV.⁴⁹ This is likely because the contribution of the emission from S_1 state become larger when ΔE is small, that is, E_{S_1} and E_{CT} are close. More specifically, the local excitation (LE) and CT states would be hybridized, which results in enhancement of EQE_{EL} as the oscillator strength of the S_1 state is generally fairly larger than that of the CT state.⁴⁹⁻⁵² Overall, minimizing ΔE is essential issue for the reduction of all the factors for E_{loss} .

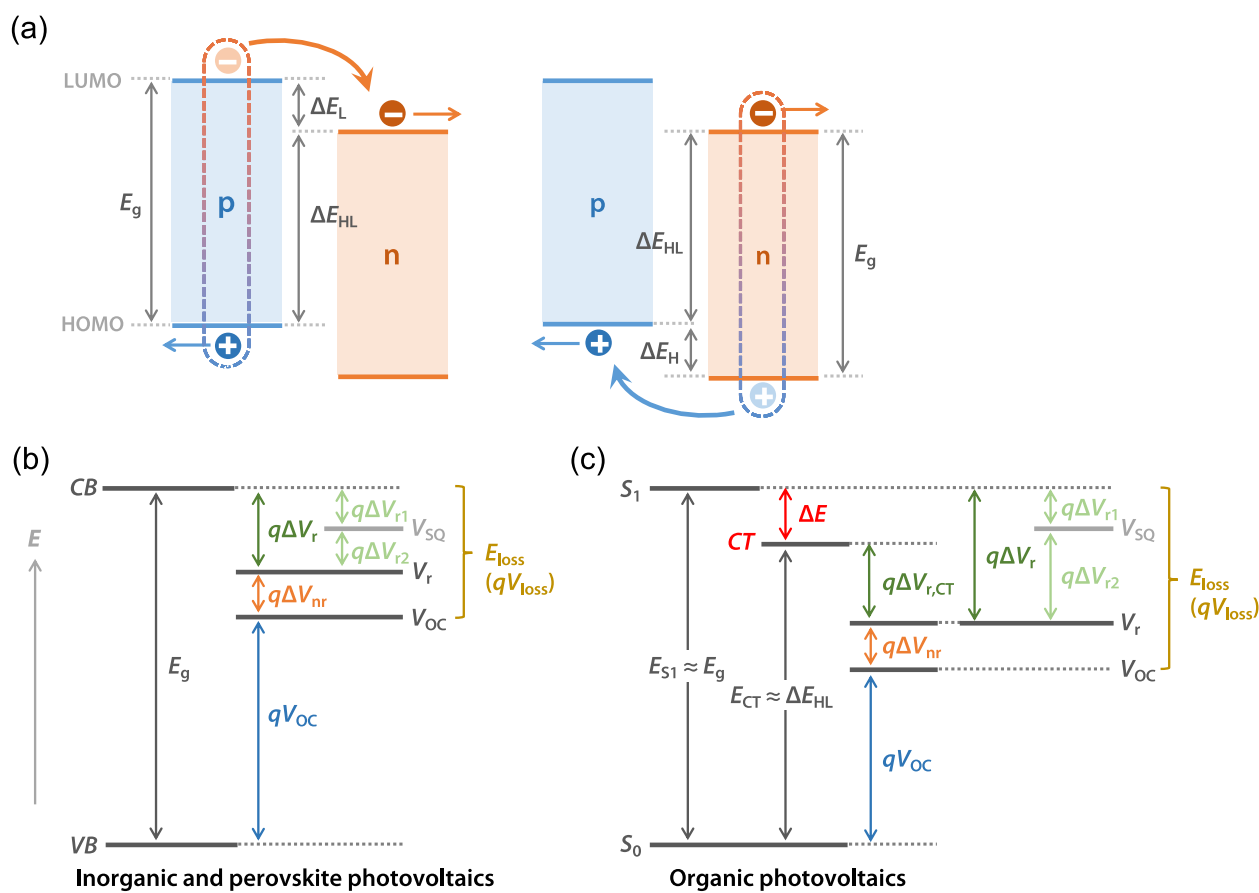


Figure 2. (a) Energy level diagrams of pairs of p-type and n-type organic semiconductors and the working principle of OPVs, when the p-type material has a narrower bandgap (E_g) (left) and the n-type material has a narrower E_g (right). (b) Relationship between the input energy (E_g) and the energy of output voltage including the factors of voltage loss and V_{OC} for inorganic and perovskite photovoltaics. Note that VB and CB are valence band and conduction band, respectively, and V_{SQ} is the maximum voltage based on the SQ limit and V_r is the upper limit of the photovoltage when only the loss due to radiative recombination is present.^{53,54} (c) Relationship between the input energy based on the state energy (Jablonski) diagram of an organic semiconductor blend and output voltage energy for OPV. $qV_{r,CT}$ and qV_r are the radiative recombination loss based on E_{CT} and E_g , respectively. (b,c) Note that voltage loss due to current (J_{SC}) loss is typically negligibly small and hence is ignored for simplicity here (see the Supporting Information).

3. Determination of E_{loss} and offset energies

The E_{loss} value is calculated by $E_g - qV_{\text{OC}}$, in which for OPVs E_g is the bandgap of the material with a narrower bandgap in the blend system. Here, it should be noted that how to determine the E_g affects the E_{loss} value.^{43,55} **Figure 3** shows different methods for determining the E_g extracted from the reference.⁵⁵ The most commonly used E_g values are determined from the onset of the UV–vis absorption spectrum, which is referred to as the optical bandgap. This method often includes some errors especially when there is no strict linear region in the absorption edge or when the light scattering is very significant for the absorption tail. Further, absorption onset of the material sometimes significantly shifts when blended with other material. Thus, in such case the absorption spectrum, or EQE spectrum, of the blend film should be used for the extraction of E_g rather than the that of the neat film (**Figure 3a**).⁵⁶ Another method for estimating E_g , which is physically meaningful, is to use the intersection of the normalized absorption and photoluminescence (PL) spectra (**Figure 3b**).^{57,58} This can be replaced by using the photovoltaic EQE spectrum and the EL spectrum of the neat device.⁴³ The use of the photovoltaic EQE spectrum of the blend system could be even better method because it represents the external property of the complete photovoltaic cell and it is accessible to every researcher who works on OPVs. E_g can be determined by the crossing point of extrapolated line of the EQE edge and horizontal tangent of the local peak (**Figure 3c**), or determined by using the inflection point of the EQE curve (**Figure 3d**),^{55,58}

For example, we here show variation of E_g in a π -conjugated polymer PNOz4T, which gives small E_{loss} when paired with [6,6]-phenyl-C₇₁-butyric acid methyl ester (PC₇₁BM) as will be described in section 4.2, by above-mentioned methods in **Table 1**. The E_g for PNOz4T was determined to be 1.54 eV from the onset of UV–vis absorption spectrum of the neat film. Whereas the E_g was determined to be 1.52 eV from the onset of the EQE spectrum for the PNOz4T/PC₇₁BM cell (method shown in **Figure 3a**), it was determined to be 1.60 eV from the EQE edge (method shown in **Figure 3c**). By

using the intersection of the UV–vis absorption and PL spectra of the neat film (method shown in **Figure 3b**), the E_g was determined to be 1.60 eV. Further, the E_g was determined to be 1.55 eV from the inflection point of the EQE spectrum (method shown in **Figure 3d**). As such, the E_g varied from 1.52 to 1.60 eV depending on the measuring methods in this case.

Note that however, E_g values shown in this review are optical bandgaps determined from the onset of the film absorption spectrum, unless otherwise noted, although we now know that this method is not the better one in terms of reproducibility and physical meaning. This is because in most of the reported studies, E_g is determined in this method. Thus, we note that the E_{loss} values shown here would include some experimental errors.

The offset energies ΔE_L and ΔE_H are often determined on the basis of the LUMO and HOMO energy levels (E_{LUMO} and E_{HOMO}) of the material that are measured separately in the neat film most typically by cyclic voltammetry (CV). In some cases, E_{LUMO} and E_{HOMO} are evaluated by low-energy inverse photoemission spectroscopy^{59,60} and photoemission spectroscopy, respectively. However, the estimation of the ΔE_L and ΔE_H values based on the E_{HOMO} and E_{LUMO} evaluated by the measurements of the isolated materials is considered to neglect the influence of exciton binding energy and other interfacial effects.⁶¹ Alternatively, the offset energy can be determined by the measurements of the blend film, in which offset energy of $\Delta E = E_g - E_{\text{CT}}$ is used. E_{CT} can be determined by the intersection of the reduced photovoltaic EQE spectrum and the reduced EL spectrum of the OPV cell (**Figure 4**).^{43, 54} Although the use of the blend film to estimate the E_{CT} is a more accurate method to determine the offset energy, the use of the neat film to estimate the energy levels is much more common in literatures, most likely because it is easier and more accessible. Thus, the offset energy values for the blend systems shown in this review are basically determined by the offset of the E_{LUMO} or E_{HOMO} , and the values should include experimental errors.

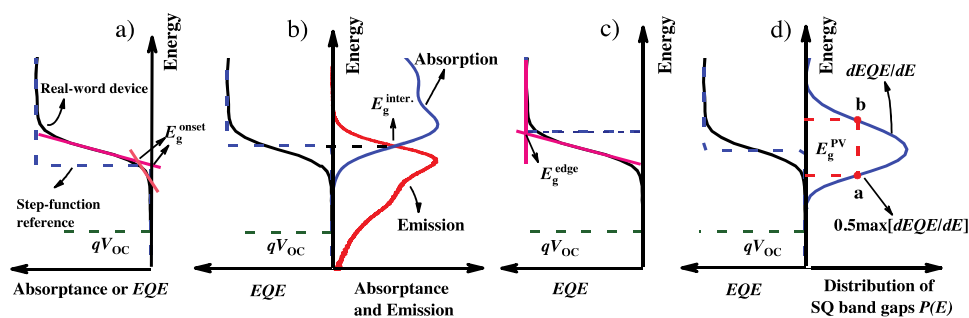


Figure 3. Different E_g determination methods. The step-functions (blue dash curves) are used as references for the absorbance or EQE (solid black curves) of real-word OSCs. a) E_g is determined from the absorbance or EQE onset. b) E_g is determined at the intersection between absorption (solid blue curve) and emission (solid red curve). c) E_g is determined from the crossing point of extrapolated line of the EQE edge and horizontal tangent of the local peak. d) E_g is determined from the inflection point of the EQE curve. Adapted with permission from reference 55. Copyright 2018, Wiley-VCH.

Table 1. E_g values for PNOz4T neat film or PNOz4T/PC₇₁BM blend film determined by different methods shown in Figure 3.

Method	Sample	E_g (eV) ^a
Onset of Abs	Neat	1.54
Onset of EQE (Figure 3a)	Blend	1.51
Intersection of Abs and PL (Figure 3b)	Blend	1.60
Edge of EQE (Figure 3c)	Blend	1.60
Inflection of EQE (Figure 3d)	Blend	1.55

a) see **Figure S2** for the experimental data for PNOz4T and PNOz4T/PC₇₁BM films.

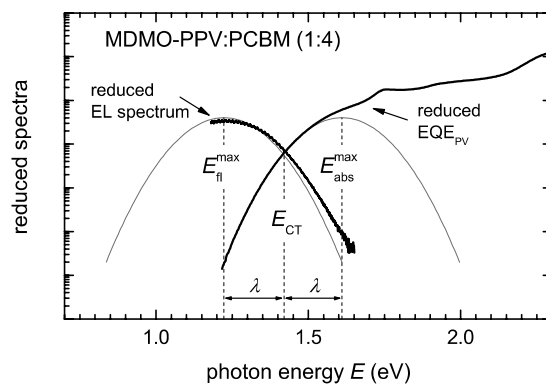


Figure 4. Determination method for E_{CT} : E_{CT} is determined at the intersection between reduced photovoltaic EQE ($E_{QE_{PV}}$) and EL spectra. The figure shows the example for an MDMO-PPV:PC₆₁BM (1:4) photovoltaic device, which is reproduced from reference 54. Copyright 2010, The American Physical Society.

4. Polymer/fullerene cells

4-1. Fullerene derivatives as n-type materials

Polymer/fullerene blends are the most widely studied systems in OPVs, in which methanofullerenes, [6,6]-phenyl-C₆₁-butyric acid methyl ester (PC₆₁BM)⁶² and PC₇₁BM (**Figure 5a**),⁶³ are commonly used as the n-type material. When one of the most common polymers, regioregular poly(3-hexylthiophene) (P3HT) (**Figure 5b**), having an E_g of around 1.9 eV, is combined as the p-type semiconductor, the cell typically shows PCEs in the range of 3–4% with V_{OC} s of around 0.6 V,⁶⁴⁻⁶⁷ resulting in the E_{loss} of ~1.3 eV. As fullerenes are n-type semiconductors, their LUMO energy levels (E_{LUMOS}) are an important parameter in discussing the E_{loss} . Thus, we here summarize fullerene derivatives that possess shallower E_{LUMOS} than PC₆₁BM and PC₇₁BM (PCBMs).⁶² Note that as most of the E_{loss} values were not discussed in the literature, we calculated the E_{loss} values shown below, using $E_g - qV_{OC}$. **Figure 5** display the chemical structures of the fullerene derivatives introduced here along with p-type semiconducting materials, and **Table 1** summarizes the electronic and photovoltaic properties of the fullerene derivatives.

The addition of functional groups to fullerene can reduce the π -conjugated system and thus raise the E_{LUMO} of fullerene.^{7,68,69,70} Among “PC₆₁BM multiadducts”, which are C₆₀ derivatives with two, three, or higher number of the same substituent (phenyl butyric acid methyl ester),^{71,72,73,74,75} PC₆₁BM bisadduct (bis-PC₆₁BM) (**Figure 5a**) is the most successful derivative for OPVs. Blom and co-workers reported that bis-PC₆₁BM had an E_{LUMO} of approximately -3.7 eV, which was ~0.1 eV shallower than that of PC₆₁BM.⁶⁴ The bis-PC₆₁BM cell thus afforded a V_{OC} that was higher by 0.15 V relative to that for the PC₆₁BM cell when the material was used in combination with P3HT; V_{OC} for the P3HT/bis-PC₆₁BM cell was 0.73 V, whereas that for the P3HT/PC₆₁BM cell was 0.58 V. As a result, E_{loss} was reduced to 1.15 eV from 1.30 eV by replacing PC₆₁BM with bis-PC₆₁BM. Further, the bis-PC₆₁BM cell exhibited high J_{SC} and FF values, resulting in the PCE of 4.5%, which was approximately a factor of 1.2 larger than that of 3.8% for the PC₆₁BM cell. This suggested that the

additional functionalization of the fullerene cage in bis-PC₆₁BM had almost no negative effect on the charge-carrier properties of fullerene.

Indene-adducted fullerene derivatives were also reported to show shallower E_{LUMOS} and thus afford higher V_{OCs} for OPVs than PCBM. Laird and co-workers demonstrated that C₆₀-indene monoadduct and bisadduct afforded V_{OCs} of 0.63 and 0.84 V, respectively, in the cells combined with P3HT,⁷⁶ were higher by 0.05 and 0.26 V, respectively, than that for the P3HT/PC₆₁BM cell of 0.58 V. The PCE was 3.9 and 5.1% for the cell with the C₆₀-indene monoadduct and bisadduct, respectively, and, in particular, the latter was markedly enhanced relative to 3.9% for the cell with PC₆₁BM. Li et al. also reported the same C₆₀ derivatives, namely, indene-C₆₀ monoadduct and bisadduct, which were called ICMA and ICBA (**Figure 5a**), respectively.⁶⁵ Interestingly, indene addition to C₆₀ in ICMA resulted in a negative shift of the reduction potential in CV, and the second addition of indene to C₆₀ in ICBA induced a stronger negative shift of the reduction potential. The E_{LUMO} values of ICMA and ICBA are, respectively, 0.05 and 0.17 eV higher than that of PCBM. Further, P3HT/ICMA and P3HT/ICBA cells showed V_{OC} values of 0.63 and 0.84 V, respectively, which were 0.05 and 0.26 V higher, respectively, than that of the P3HT/PC₆₁BM cell of 0.58 V reported in the same literature. As a result, the E_{loss} values for the ICMA and ICBA cells were calculated to be 1.25 and 1.04 eV, respectively. Although the values were still large, the E_{loss} for the ICBA cell was significantly smaller than that for the PC₆₁BM cell.

Nakamura and co-workers developed and evaluated bis(dimethylphenylsilylmethyl)[60]fullerene (SIMEF) (**Figure 5a**) as an n-type fullerene derivative.⁷⁷ SIMEF had an E_{LUMO} of -3.70 eV, which was approximately 0.2 eV higher than that of PC₆₁BM. The P3HT/SIMEF cell showed a higher V_{OC} (0.67 V) than the P3HT/PC₆₁BM cell (0.58 V), with the E_{loss} of the former being 1.23 eV.⁷⁸ In addition, when SIMEF was combined with tetrabenzoporphyrin (BP) (**Figure 5b**), which was thermally converted from the corresponding precursor, as the p-type material, the resultant cell showed a V_{OC} of 0.75 V, which was 0.2 V higher than that for the PC₆₁BM cell, along with a PCE of 5.2%. In this case, the E_{loss} for the BP/SIMEF cell was calculated to be 0.97 eV.⁷⁷

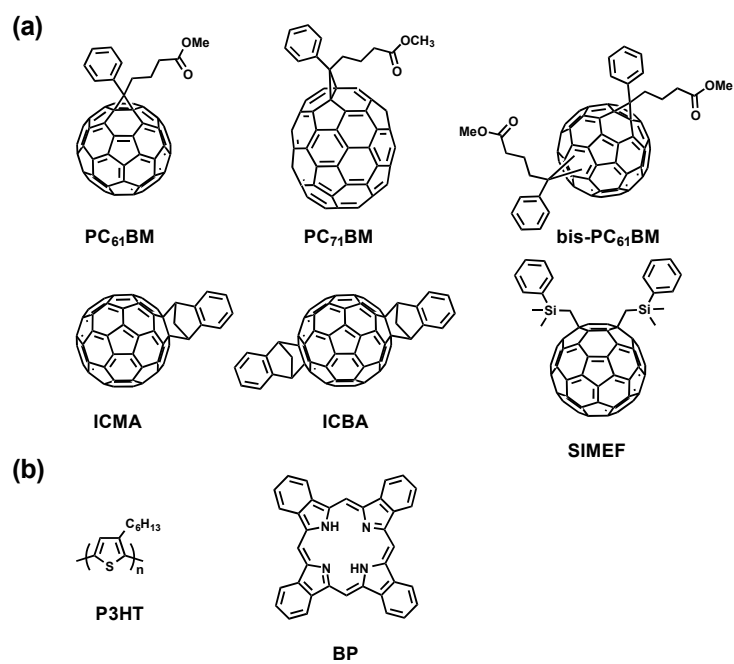


Figure 5. (a) PCBMs and C₆₀-fullerene derivatives with shallow LUMO energy levels. (b) p-Type materials combined with these fullerene materials in the OPV cell.

Table 1. Electronic and photovoltaic properties of fullerene derivatives

Fullerene	E_{LUMO} (eV) ^a	p-type/ E_{g} (eV) ^b	ΔE_{L} (eV)	EQE_{max} (%)	J_{SC} (mA cm ⁻²)	V_{OC} (V)	FF	PCE_{max} (%)	E_{loss} (eV)	ref
PC ₆₁ BM	-3.91	P3HT / 1.88	~1.1 ^d	65 ^e	10.8	0.58	0.66	3.9	1.30	66
bis-PCBM	-3.71	P3HT / 1.88	~0.86 ^d	70 ^e	9.1	0.73	0.68	4.5	1.15	64
ICMA	-3.86	P3HT / 1.88	~1.0 ^d	–	9.7	0.63	0.64	3.9	1.25	65
ICBA	-3.74	P3HT / 1.88	~0.89 ^d	62 ^e	9.7	0.84	0.67	5.4	1.04	65
SIMEF	-3.70	P3HT / 1.88	~0.85 ^d	63 ^e	9.8	0.67	0.52	3.2	1.23	78
		BP / 1.72	–	49 ^e	10.5	0.75	0.65	5.2	0.97	77

a) LUMO energy levels determined by CV. b) p-type semiconducting material combined in the photovoltaic cell/optical bandgap of the p-type material. d) E_{L} for P3HT was assumed to be -2.85 eV, which was estimated using CV by the authors of this review. e) maximum EQE value extracted from the EQE spectrum in the corresponding literature by the authors of this review.

4-2. π -Conjugated polymers as p-type materials

One of the most highly performing π -conjugated polymers in polymer/fullerene systems is PTB7-Th (**Figure 6**), which is also called PBDTTT-EFT or PCE10.⁷⁹ The PTB7-Th/PC₇₁BM system generally gives PCEs of around 9% with a V_{OC} of 0.78 V.^{79, 80} As the E_g for PTB7-Th is 1.58 eV, the E_{loss} for the PTB7-Th/PC₇₁BM system is as large as 0.80 eV. This means that there is much room for reducing the E_{loss} for polymer/fullerene systems. In order to realize this, fine tuning of the energetics of the p-type π -conjugated polymers with respect to those of PCBM is a promising strategy as tuning of the energetics of fullerenes has limitations and, so far, fullerenes other than PCBM are not a good pair to the polymers other than P3HT. π -Conjugated polymers enabling a small E_{loss} should be designed with a strong electron-deficient heteroaromatic ring (acceptor) as the building unit in the backbone, so that the E_{LUMO} can be effectively deepened to reduce the ΔE_L . Here, we introduce D–A polymers that incorporate a range of strong acceptor units, affording deep E_{LUMOs} . The chemical structures of the polymers described here are shown in **Figure 6**. The electronic and photovoltaic properties of the polymers are summarized in **Table 2**.

Bazan and co-workers reported a D–A polymer, PIPCP (**Figure 6**), which is composed of pyridylthiadiazole (PT) as the strong acceptor unit and cyclopentadithiophene (CDT) and indacenodithiophene (IDT) as the electron-rich donor unit.²⁹ The E_{LUMO} of PIPCP was determined to be -3.74 eV by adding E_g of 1.46 eV to the E_{HOMO} of -5.21 eV estimated by CV. A high V_{OC} of 0.86 V, considering the narrow E_g of the polymer, was observed for the PIPCP/PC₆₁BM cell, which resulted in a small E_{loss} of 0.60 eV. Further, the PIPCP/PC₆₁BM cell exhibited as high as 6.1% PCE with the EQE_{max} of 62%, which was higher than that for OPVs with a small E_{loss} of around 0.6 eV. They further studied the polymer system in depth and found that the E_g of PIPCP in the blend film was determined to be 1.41 eV by photothermal deflection spectroscopy. With the improved V_{OC} of 0.89 V, the E_{loss} was re-estimated to be 0.52 eV.⁵⁶ They assumed that the high morphological order and the low energetic disorder in the PIPCP/PC₆₁BM blend film, as proven by the small Urbach energy (E_U) of 27 meV, would account for the minimized E_{loss} .

Janssen et al. designed a series of π -conjugated polymers incorporating thiazole-flanked diketopyrrolopyrrole (DPP) as the acceptor unit with different donor units, such as thiophene (PDPP2TzT), benzodithiophene (PDPP2TzBDT), bithiophene (PDPP2Tz2T), and dithienopyrrole (PDPP2TzDTP) (**Figure 6**).³² Introducing the thiazole rings next to the DPP moiety further deepened the E_{LUMOS} compared with those of typical DPP-based polymers in which the thiophene rings are typically attached to the DPP unit. As a result, ΔE_{LUMO} , the offset energy of LUMO between the p-type and n-type materials, was determined to be 0.07–0.22 eV from the difference in reduction potential between the polymer and PC₇₁BM in CV, and this, in turn, resulted in very small E_{loss} values of 0.48–0.59 eV. It was also found that the EQE_{max} decreased with the decrease of ΔE_{LUMO} . The PDPP2TzT/PC₇₁BM cell with the smallest E_{loss} of 0.48 eV showed a low PCE of 1.1% because of its low EQE_{max} of 5% and thus low J_{SC} of 2.0 mA cm⁻², which was ascribable to its very small ΔE_{LUMO} of 0.07 eV. The other polymers showed high PCEs relative to PDPP2TzT due to the increased EQE_{max} and J_{SC} s; PCEs were 3.2% ($E_{\text{loss}} = 0.55$ eV, EQE_{max} = 25%) for PDPP2TzBDT/PC₇₁BM, 5.1% ($E_{\text{loss}} = 0.55$ eV, EQE_{max} = 40%) for PDPP2Tz2T/PC₇₁BM, and 5.6% ($E_{\text{loss}} = 0.59$ eV, EQE_{max} = 52%) for PDPP2TzDTP/PC₇₁BM cells, respectively.

Owing to the high electronegativity, the introduction of a fluorine atom can effectively deepen the E_{LUMOS} of the π -conjugated polymers.^{81,82,83,84} Among a number of fluorinated polymers, a series of polymers based on the emerging strong acceptor unit naphthobisthiadiazole (NTz) are a good example for studies of the E_{loss} reduction. An NTz-based polymer having a quaterthiophene donor unit (PNTz4T) (**Figure 6**),¹⁹ which has an E_{g} of 1.56 eV, exhibited a PCE of 10.1% for the cell combined with PC₇₁BM.⁸⁵ However, because the V_{OC} was limited to 0.71–0.74 V, the E_{loss} for the PNTz4T cell was 0.82–0.85 eV, which was the typical range for polymer/fullerene cells. Osaka and co-workers synthesized a series of NTz-based polymers by introducing fluorine atoms on the bithiophene moiety and/or the NTz unit (**Figure 6**).^{86,87} When fluorine atoms were introduced on the bithiophene moiety (F0-F2 and F0-F4), the E_{HOMOS} were downshifted more than the E_{LUMOS} , resulting in large E_{g} values.⁸⁶ On the other hand, when fluorine atoms were introduced on the NTz unit (F2-

F0), the E_{LUMO} was downshifted more than the E_{HOMO} , resulting in a narrow E_{g} .⁸⁷ This could be explained by the geometry of HOMOs and LUMOs, where HOMOs are mainly located on the quaterthiophene unit and LUMOs are mainly located on the NTz moiety. Note that because F2-F2 had fluorine atoms on both the bithiophene unit and the NTz unit, both E_{HOMO} and E_{LUMO} were equally downshifted, which resulted in a similar E_{g} to PNTz4T. As a consequence, the E_{loss} was successfully reduced in all cases; 0.78 eV for F0-F2, 0.69 eV for F0-F4, 0.73 eV for F2-F0, and 0.69 eV for F2-F2. The F2-F2 cell showed the best performance with up to 10.8% PCE, along with the smallest E_{loss} among these polymers.

Yu et al. reported a benzo[1,2-*b*:4,5-*b'*]dithiophene (BDT)-based polymer named PBDTT-SF-TT (**Figure 6**), in which the alkyl group on the thiophene substituents of PTB7-Th was replaced with an alkylthio group, leading to deeper energy levels.⁸⁸ In fact, the E_{HOMO} of PBDTT-SF-TT was found to be -5.54 eV, which was deeper by 0.24 eV than that of PTB7-Th, whereas the E_{g} of 1.59 eV was similar. The V_{OC} for the PBDTT-SF-TT/PC₇₁BM cell was 1.0 V, which was higher by more than 0.2 V than that for the PTB7-Th/PC₇₁BM cell of 0.78 V. Thus, the E_{loss} was significantly reduced to 0.59 eV from 0.80 eV. Importantly, the PCE remained high at 9.1%, whereas the PTB7-Th cell showed 9.0% PCE.

Naphthobisoxadiazole (NOz), an oxygen analog of NTz, is a very strong acceptor unit due to the high electronegativity of oxygen.⁸⁹ Osaka and co-workers reported that an NOz-based polymer (PNOz4T) (**Figure 6**) had an E_{LUMO} of -3.65 eV, which is deeper than that of PNTz4T by ca. 0.2 eV, resulting in a very small ΔE_{LUMO} of 0.12 eV, which is much smaller than the empirical threshold value of 0.3 eV. This was further confirmed by the EL measurement of the PNOz4T/PC₇₁BM device, which showed a very similar spectrum to the PL spectrum of PNOz4T, suggesting that the E_{S1} and the E_{CT} are very close and thus the offset energy is nearly 0 eV. As a result, the PNOz4T/PC₇₁BM cells exhibited remarkably high V_{OC} s of up to ~ 1 V despite the fact that the polymer had a small E_{g} of 1.54 eV, leading to significantly small E_{loss} values of 0.54–0.58 eV.³⁰ Those values were among the smallest for polymer/PCBM-based cells, smaller than the empirical limit of 0.6 eV. Importantly,

those cells exhibited EQE_{max} of 65% and as high as 8.9% PCEs despite the small ΔE_{L} . Further, a transient absorption spectroscopy study revealed that the charge dissociation was almost 100% and the EQE was limited by the exciton diffusion, which implied that the small driving-force energy would not be a limiting factor for the charge generation. A striking feature of PNOz4T is its very high crystallinity in the thin film and the high charge carrier mobility of $1 \text{ cm}^2 \text{ V}^{-1} \text{ s}^{-1}$ in the transistor device. In addition, the E_{U} estimated from the EQE spectra of both neat and blend films were 27 meV (**Figure S2**), suggesting that the polymer is highly ordered and that EQE corresponding to the CT absorption is negligible. It is speculated that the high charge transport would facilitate the charge generation and thus prevent the geminate recombination at the p/n interface that could more easily happen when the ΔE_{L} is small. Gao and co-workers reported that the $q\Delta V_{\text{nr}}$ for the PNOz4T/PC₇₁BM cell was 0.24 eV, which was significantly smaller than that for the common PTB7-Th/PC₇₁BM cell and similar to that for polymer/non-fullerene acceptor (NFA) cells with small E_{loss} values. This was another reason for the small E_{loss} in this system.⁴⁹ Such a small $q\Delta V_{\text{nr}}$ is probably because of LE-CT hybridization due to negligibly small ΔE_{L} , as theoretically suggested.⁴⁷

Wong, Chou, and co-workers also reported the development of an NOz-based polymer (PSiNO) (**Figure 6**), in which a silole-based ladder-type fused ring was combined as the donor unit.⁹⁰ PSiNO had an E_{g} of 1.56 eV. Although they did not discuss the E_{loss} issue in their report, the PSiNO/PC₇₁BM cell exhibited a high V_{OC} of 0.90 V, thus the E_{loss} was calculated to be 0.66 eV, and a relatively high PCE of 8.4%.

Guo, Facchetti, and co-workers synthesized copolymer PISOBBT4T (**Figure 6**) based on benzo[1,2-*d*:4,5-*d'*]bis[1,2,3]-thiadiazole (isoBBT),⁹¹ a regioisomer of the widely studied benzobis[1,2-*c*:4,5-*c'*]bis[1,2,5]thiadiazole (BBT) unit. The isoBBT unit was found to downshift the E_{HOMO} and upshift the E_{LUMO} with respect to the BBT unit. Thus, PISOBBT4T had an E_{g} of 1.40 eV, which was significantly wider than that of the BBT counterpart, with deep E_{LUMO} and E_{HOMO} of approximately -3.9 eV and -5.4 eV (determined by $E_{\text{LUMO}} - E_{\text{g}}$), respectively. The

PisoBBT4T/PC₆₁BM cell gave a V_{OC} of 0.81 V, which resulted in an E_{loss} of 0.59 eV, and a PCE of 10.3% that is relatively high for fullerene-based cells.

4-3. Summary

In polymer/fullerene-based devices, multifunctionalized fullerene derivatives with a shallower E_{LUMO} have led to a smaller ΔE_L , thereby reducing the E_{loss} when combined with P3HT. However, the E_{loss} values are still around 1 eV due to the very shallow E_{LUMO} of P3HT and thus the large ΔE_L s of more than 0.8 eV in all cases. Unfortunately, no good performance has been reported so far for these shallow E_{LUMO} fullerene derivatives with the combination of D–A polymers with narrower E_{gs} , likely due to the increased population of the triplet state in the fullerene derivatives.^{92,93} On the other hand, the development of new π -conjugated polymers incorporating a very strong acceptor unit has realized the reduction of ΔE_L and thus E_{loss} to below 0.6 eV, a minimum value that had previously been suggested for OPVs. Some systems were found to have an E_{loss} even close to 0.5 eV, which is comparable to that for inorganic solar cells. Although polymer/fullerene-based devices showed significantly decreased EQE_{max} when the E_{loss} was less than 0.6 eV, exceptionally PIPCP and PNOz4T showed relatively high EQE_{max} s even with the small E_{loss} values. This is partly because of LE–CT hybridization due to negligibly small ΔE_L . Although the reason is not yet fully understood, a common feature in these polymers is the highly ordered structure in the blend film, which most likely originates in the π -extended large fused ring systems that are used as the building unit for their polymer backbones. Such structural feature could be a key factor for achieving efficient charge generation under a small driving-force energy.

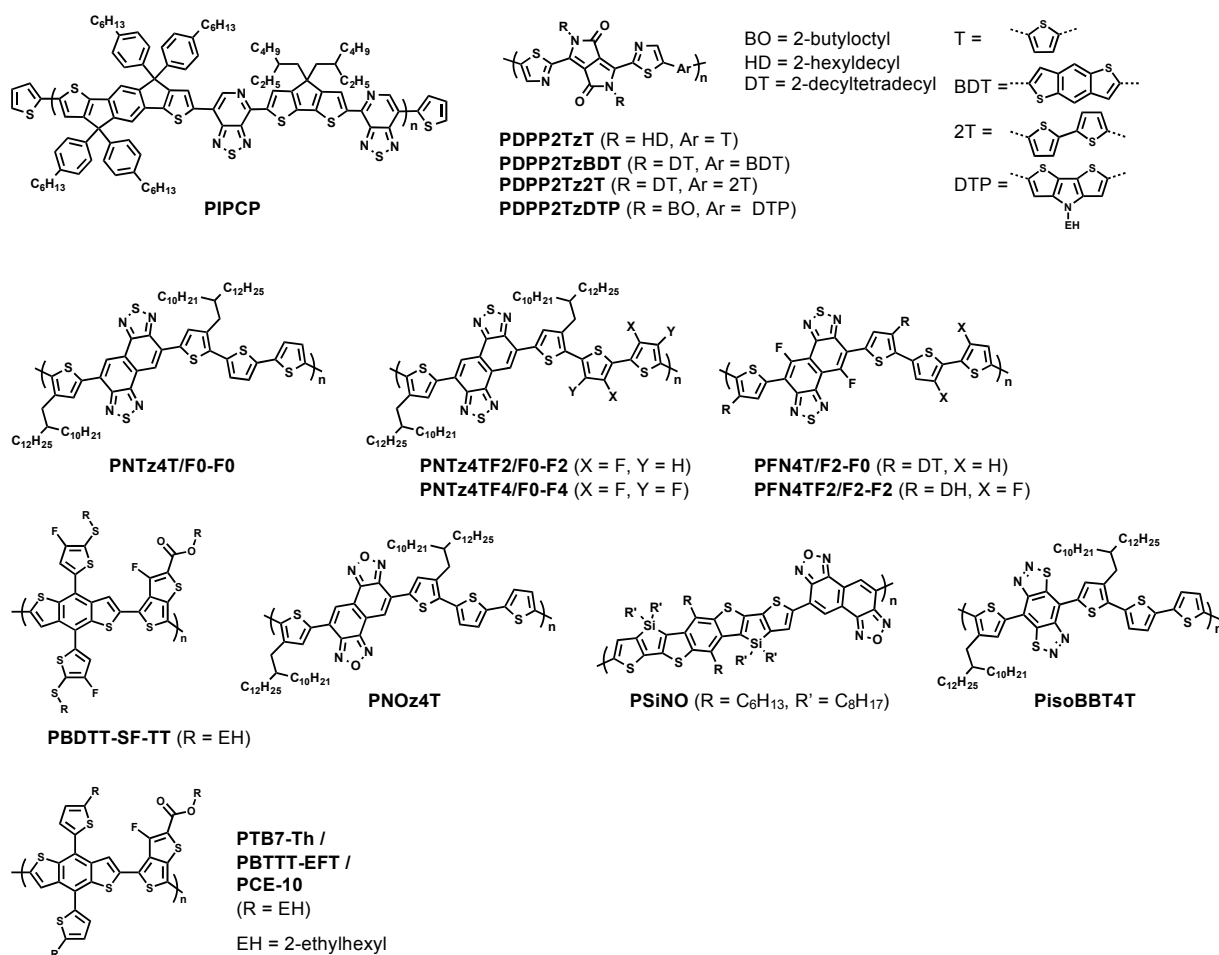


Figure 6. Narrow-bandgap π -conjugated polymers reported to show small E_{loss} values in combination with PCBM. A standard polymer PTB7-Th is also shown.

Table 2. Electronic and photovoltaic properties of narrow-bandgap π -conjugated polymers as p-type material enabling small E_{loss}

Narrow-bandgap Polymer	E_g (eV) ^a	$E_{\text{HOMO}}/E_{\text{LUMO}}$ (eV) ^b	fullerene ^c	ΔE_L (eV)	EQE_{max} (%)	J_{SC} (mA cm ⁻²)	V_{OC} (V)	FF	PCE_{max} (%)	E_{loss} (eV)	ref
PIPCP	1.46	-5.21/ -3.74 ^d	PC ₆₁ BM	–	62 ^e	13.4	0.86	0.53	6.1	0.60	29
PDPP2TzT	1.44	-5.54/ -3.64	PC ₇₁ BM	0.07	5	2.0	0.96	0.58	1.1	0.48	32
PDPP2TzBDT	1.53	-5.51/ -3.57	PC ₇₁ BM	0.16	25	6.2	0.98	0.53	3.2	0.55	32
PDPP2Tz2T	1.47	-5.46/ -3.52	PC ₇₁ BM	0.21	40	8.8	0.92	0.63	5.1	0.55	32
PDPP2TzDTP	1.28	-5.18/ -3.51	PC ₇₁ BM	0.22	52	14.9	0.69	0.54	5.6	0.59	32
PNTz4T (F0-F0)	1.56	-5.20/ -3.46	PC ₇₁ BM	0.31	79	19.4	0.71	0.73	10.1	0.85	19
PNTz4TF2 (F0-F2)	1.60	-5.42/ -3.49	PC ₇₁ BM	0.28	82	19.3	0.82	0.67	10.5	0.78	86
PNTz4TF4 (F0-F4)	1.62	-5.49/ -3.56	PC ₇₁ BM	0.21	51	10.5	0.93	0.66	6.5	0.69	86
PFN4T (F2-F0)	1.46	-5.25/ -3.55	PC ₇₁ BM	0.22	71	19.2	0.73	0.68	9.6	0.73	87
PFN4TF2 (F2-F2)	1.53	-5.48/ -3.60	PC ₇₁ BM	0.17	73	17.8	0.84	0.72	10.8	0.69	87
PBDTT-SF-TT	1.59	-5.54/ -3.95 ^d	PC ₇₁ BM	–	82	14.8	1.00	0.61	9.1	0.59	88
PNOz4T	1.52	-5.48/ -3.65	PC ₆₁ BM	0.12	65	14.0	0.98	0.64	8.7	0.54	30
			PC ₇₁ BM	0.12	63	14.5	0.96	0.64	8.9	0.56	30
PSiNO	1.56	-5.50/ -3.73 ^d	PC ₇₁ BM	–	62 ^e	13.3	0.90	0.70	8.4	0.66	90
PisoBBT4T	1.40	-5.43/ -4.03	PC ₆₁ BM	–	68 ^e	20.8	0.81	0.61	10.3	0.59	91
PTB7-Th	1.58	-5.24/ -3.66	PC ₇₁ BM	–	71 ^e	16.9	0.78	0.68	9.0	0.80	79

a) Optical bandgap determined from the absorption onset. b) HOMO and LUMO energy levels determined by CV. c) fullerene material combined in the photovoltaic cell. d) LUMO energy level calculated by the addition of E_g to the HOMO energy level based on CV. e) maximum EQE value extracted from the EQE spectrum in the corresponding literature by the authors of this review.

5. Polymer/non-fullerene cells

5-1. Non-fullerene n-type materials (Non-fullerene acceptors: NFAs)

Non-fullerene n-type organic semiconductors, namely, non-fullerene acceptors (NFAs), are state-of-the-art materials in the OPV area. NFAs can be classified by their bandgaps, *i.e.*, NFAs with wide bandgaps of more than 2 eV and those with narrow bandgaps of less than 1.8 eV. Wide-bandgap NFAs are combined with p-type polymers having narrow bandgaps, and thus the E_{loss} is correlated to the ΔE_{L} . Narrow-bandgap NFAs, on the other hand, are typically combined with wide-bandgap p-type polymers, and thus the E_{loss} is correlated to the ΔE_{H} , although in some cases they are combined with narrow-bandgap polymers. In this section, we summarize NFAs with wide and narrow bandgaps (**Figures 7 and 8**, respectively). We also present some important wide-bandgap p-type polymers that are typically combined with narrow-bandgap NFAs (**Figure 9**). The electronic and photovoltaic properties of the NFAs and the polymers are summarized in **Tables 3, 4, and 5**, respectively.

5-1-1. Wide-bandgap NFAs

Perylene diimide (PDI), a well-known dye molecule, is the most commonly used building unit for wide-bandgap NFAs due to its absorption property and electron-deficient nature.^{46,94,95} In early studies of NFAs, simple PDI derivatives with substituents at the *N*-position were investigated.⁹⁶⁻⁹⁸ However, most likely due to their nearly planar structure, those PDI derivatives form aggregates in the blend film, which results in very poor performances in the OPV cells. On the other hand, recently, PDI-based NFAs in which multiple PDI or related building units are linked in twisted manners have been designed in order to hinder such strong aggregation. Further, the twisted geometries would result in the localization of the π -conjugation at each building unit, which would lead to a wide bandgap and a shallow E_{LUMO} .

Yan and co-workers reported two PDI-based NFAs, diPDI and SF-PDI2 (**Figure 7a**). In diPDI, two *N,N*-dialkyl PDIs are directly linked to be dimerized, whereas in SF-PDI2, the two PDI units are attached to spirobifluorene.⁹⁹ Although the absorption spectra and the E_{g} s of the two materials were

mostly identical, both E_{HOMO} and E_{LUMO} were deeper for SF-PDI2 than for diPDI: E_{LUMO} values, determined on the basis of E_{HOMO} and E_{g} , were -3.96 eV for diPDI and -3.83 eV for SF-PDI2. These materials were paired with PffBT4T-DT (**Figure 7b**) with the E_{g} of 1.65 eV in the OPV cell. The cells demonstrated V_{OCs} of 0.84 and 0.98 V, respectively, both of which were higher than that for the PffBT4T-DT/PC₆₁BM cell by 0.2 V. As a result, the E_{loss} values for the diPDI and SF-PDI2 cells were 0.81 and 0.67 eV, respectively. SF-PDI2 was also combined with p-type polymer P3TEA (**Figure 7b**) having the E_{g} of 1.72 eV, which was determined on the basis of the crossing point between the absorption and PL spectra. The P3TEA/SF-PDI2 cell exhibited a very high V_{OC} of 1.11 V, which resulted in a small E_{loss} of 0.61 eV, and a high PCE of 9.5% .¹⁵ Interestingly, despite the small E_{loss} as well as the small ΔE_{L} of 0.05 eV, the EQE_{max} was relatively high with 66% and the maximum internal quantum efficiency (IQE_{max}) was found to be nearly 90% , which originated in the fast charge generation.

Cho and co-workers reported a related material, SF-PDI4 (**Figure 7a**), where two more PDI units were attached to the other fluorene moiety.¹⁰⁰ Thus, SF-PDI4 has a more twisted 3D conformation than SF-PDI2, which possibly further hinders aggregation in the film. SF-PDI4 has an E_{LUMO} of -3.78 eV as determined by CV. Unfortunately, this value could not be directly compared with that for SF-PDI2 because their measurement methods differed. SF-PDI4 was blended with P4T2FBT (PffBT4T-DT) and PV4T2FBT (**Figure 7b**) in OPV cells, which provided V_{OCs} of 0.93 and 0.90 V, giving rise to the E_{loss} values of 0.71 and 0.70 eV, respectively. These values were slightly larger than those for the SF-PDI2 cell. Several other PDI-based wide-bandgap NFAs with four PDI units attached to a central core unit were also reported: TPC-PDI4¹⁰¹⁻¹⁰³ with tetraphenylmethane, TPE-PDI4¹⁰³ with the tetraphenylethylene core,¹⁰⁴ and TPPz-PDI4 with the tetraphenyl pyrazine core (**Figure 7a**).¹⁰³ Those three materials were systematically investigated by blending with PffBT-T3(1,2)-2 (**Figure 7b**).¹⁰³ The E_{LUMOs} for these three materials based on CV were similar at around -3.75 , and the ΔE_{L} s were less than 0.1 eV. Interestingly, however, the V_{OCs} for the cells appeared different and the materials with a more twisted structure showed higher V_{OC} values: 1.04 V for TPC-PDI4, 1.03 V for TPE-PDI4,

and 0.99 V for TPPz-PDI4. As a result, the E_{loss} values increased as 0.59, 0.60, and 0.64 eV for TPC-PDI4, TPE-PDI4, and TPPz-PDI4, respectively, though the EQE_{max} s and the PCEs decreased in this order. The same trend was found when P3HT and PTB7-Th were employed as the p-type polymer.

Yan and co-workers designed and synthesized a PDI-based NFA named FTTB-PDI4 (**Figure 7a**) through the ring fusion of the PDI moiety with the thiophene linker on the central benzene core.¹⁰⁵ Interestingly, the ring fusion reduced the twisting of the PDI moieties, which led to the highly delocalized HOMO and LUMO densities as well as the highly developed π -conjugation throughout the molecular structure. The E_{LUMO} for FTTB-PDI4 was -3.58 eV, which was 0.1 eV shallower than that for the precursor material before the ring fusion. This would be attributed to the electron-donating nature of the thiophene moiety incorporated by the ring fusion. Further, the ΔE_{L} value for the blend of FTTB-PDI4 with P3TEA was negligibly small at 0.02 eV, which led to a markedly high V_{OC} of 1.13 V and thus a small E_{loss} of 0.53 eV. Despite the negligible ΔE_{L} , interestingly, the OPV cell based on the blend exhibited a high EQE_{max} of 68% and thus a PCE of 10.6%.

Apart from the PDI-related wide-bandgap NFAs, McCulloch and co-workers reported a series of rhodanine-end-capped rigid-rod NFAs.^{18, 106} Among them, FBR (**Figure 7a**), in which bisbenzothiadiazolyfluorene was used as the core structure, had a wide E_{g} of around 2 eV, probably arising from the twisted linkage between the benzothiadiazole and fluorene units, and a relatively deep E_{LUMO} of -3.75 eV, being suitable for narrow-bandgap p-type polymers. When PffBT4T-DT with the E_{g} of 1.61 eV was paired, the blend had a very small ΔE_{L} of 0.05 eV. Consequently, the cell showed a high V_{OC} of 1.12 V, which led to a significantly small E_{loss} of 0.49 eV. The EQE_{max} was relatively high as 57% for such a small E_{loss} and the PCE was reasonably high as 7.8%.

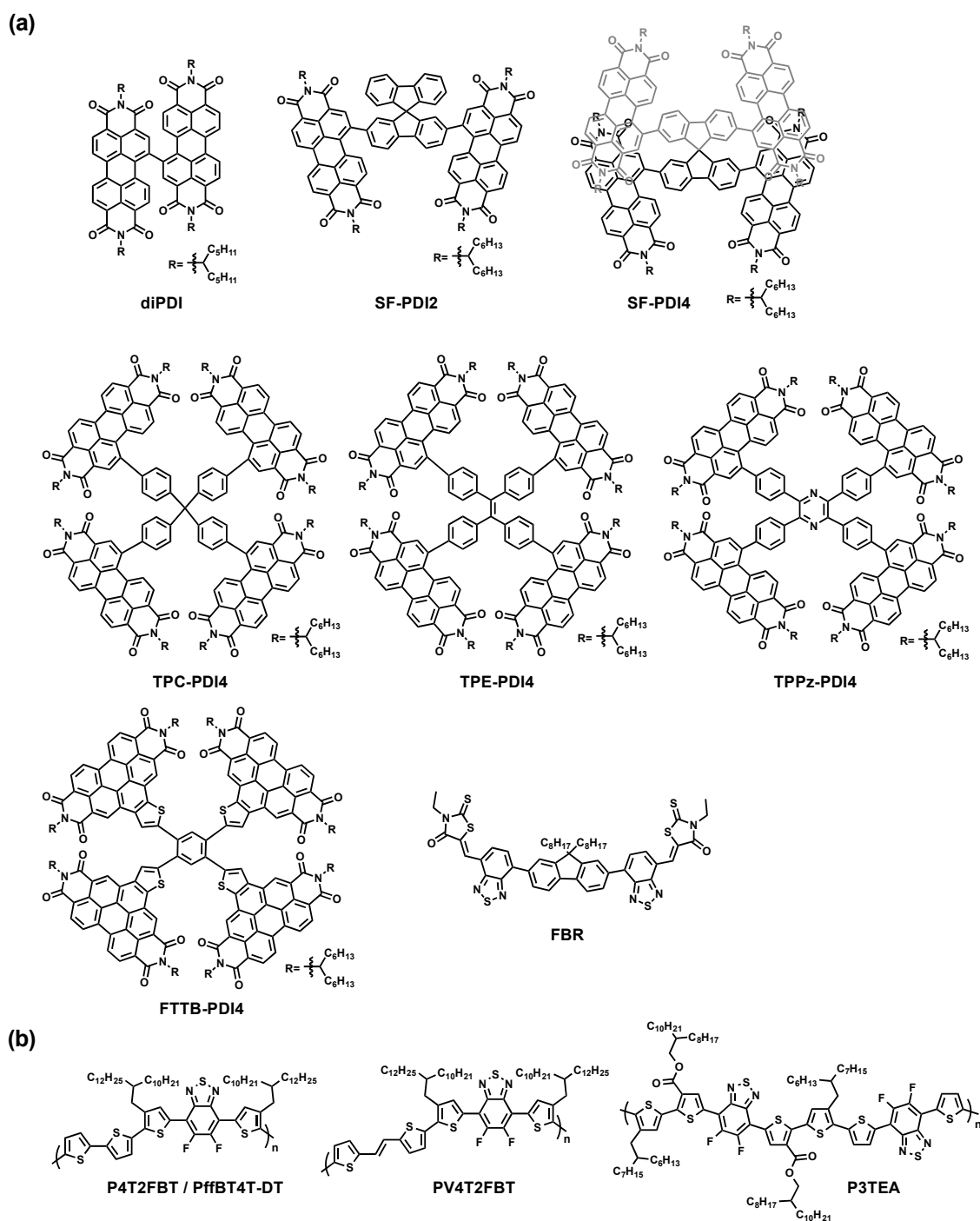


Figure 7. (a) Wide-bandgap non-fullerene acceptors. (b) Narrow-bandgap p-type polymers combined with the wide-bandgap non-fullerene acceptors.

Table 3. Electronic and photovoltaic properties of wide-bandgap non-fullerene acceptors

Wide-bandgap NFA	E_g (eV) ^a	$E_{\text{HOMO}}/ E_{\text{LUMO}}$ (eV) ^b	p-type/ E_g (eV) ^c	ΔE_L (eV)	EQE_{max} (%)	J_{SC} (mA cm ⁻²)	V_{OC} (V)	FF	PCE (%)	E_{loss} (eV)	ref
diPDI	2.10	-5.99/ -3.96	PffBT4T-DT/ 1.65	0.25	55 ^e	12.3	0.84	0.53	5.4	0.81	99
SF-PDI2	2.37	-5.90/ -3.83	PffBT4T-DT/ 1.65	0.12	51 ^e	11.1	0.98	0.57	6.3	0.67	99
			P3TEA/1.72	0.05	66	13.3	1.11	0.64	9.5	0.61	15
SF-PDI4	2.05	-5.97/ -3.78	PffBT4T-DT/ 1.64	0.28	55 ^e	11.0	0.93	0.51	5.3	0.71	100
			PV4T2FBT/ 1.60	0.27	55 ^e	12.0	0.90	0.54	6.0	0.70	100
TPC-PDI4	2.25	-5.86/ -3.75	PffBT-T3(1,2)- 2/1.63	0.07	46 ^e	8.8	1.04	0.51	4.7	0.59	103
TPE-PDI4	2.05	-5.77/ -3.72	PffBT-T3(1,2)- 2/1.63	0.04	54 ^e	11.1	1.03	0.54	6.0	0.60	103
TPPz-PDI4	2.25	-5.86/ -3.76 ^d	PffBT-T3(1,2)- 2/1.63	0.08	61	12.7	0.99	0.56	7.1	0.64	103
FTTB-PDI4	1.88	-5.74/ -3.58	P3TEA/1.72	0.02	68	13.9	1.13	0.66	10.6	0.53	105
FBR	2.10	-5.75/ -3.75	PffBT4T-DT/ 1.61	0.05	57	11.5	1.12	0.61	7.8	0.49	106

a) Optical bandgap determined from the absorption onset. b) HOMO and LUMO energy levels determined by CV. c) n-type semiconducting material combined in the photovoltaic cell. d) LUMO energy level calculated by the addition of E_g to the HOMO energy level based on CV. e) maximum EQE value extracted from the EQE spectrum in the corresponding literature by the authors of this review.

5-1-2. Narrow-bandgap NFAs

Narrow-bandgap NFAs typically have chemical structures composed of a rigid-rod π -extended fused ring as the core that is shielded by bulky non-conjugated side chains and is end-capped with polar functional groups often used as the building unit of organic dyes (**Figure 8**). The bulky side chains would offer high solubility as well as hinder aggregation that is thought to be detrimental to the photovoltaic performance. As can be seen in **Table 4**, the energy levels for the narrow-bandgap NFAs are deep, which is likely due to the strong electron deficiency of the end-capping groups.

IDTBR (**Figure 8**),^{18,106} one of the rhodanine-end-capped NFAs having IDT as the core, was reported to have a relatively narrow E_g of 1.63 eV and an E_{HOMO} of -5.45 eV. When IDTBR was blended with P3HT, the cell showed a V_{OC} of 0.72 V, giving rise to a large E_{loss} of ~ 0.9 eV, which was due to the large ΔE_{H} of ~ 0.5 eV, although the cell showed one of the highest PCEs among the P3HT-based cells, $\sim 6.3\%$.^{18,106} However, when the polymer was switched to PffBT4T-DT having a deeper E_{HOMO} of -5.34 eV than P3HT, the cell exhibited V_{OC} that was as high as 1.07 V and thus a small E_{loss} of 0.56 eV, and a relatively high PCE of 9.95%.¹⁰⁶ A similar polymer, PffBT2T-TT, was also paired with IDTBR. The cell showed a V_{OC} of 1.08 V, which resulted in a small E_{loss} of 0.55 eV. However, the cell showed a relatively high EQE_{max} of 67% and an improved PCE of 10.4%.¹⁰⁷ Interestingly, both ΔE_{H} and ΔE_{L} were similarly small at < 0.1 eV, due to nearly the same E_g for PffBT2T-TT and IDTBR.

ITIC (**Figure 8**), in which the indacenodithienothiophene (IDTT) core that is further π -extended fused ring compared to IDT, is end-capped with dicyanomethyleneindanone (DCM) groups, is one of the prototypes for emerging NFAs.¹⁴ The reported E_g , E_{HOMO} , and E_{LUMO} values for ITIC are typically 1.60, -5.61 , and -4.02 eV, respectively. When PTB7-Th having an E_g similar to ITIC was used as the p-type polymer, the ITIC-based cell had a PCE of 6.3% and a V_{OC} of 0.81 V, resulting in an E_{loss} of 0.79 eV, which was similar to that for the PTB7-Th/PC₆₁BM cell. The relatively large E_{loss} for the PTB7-Th/ITIC cell is most likely because both ΔE_{H} and ΔE_{L} are relatively large (~ 0.3 eV).

The use of PBDB-T having a wider E_g and a deeper E_{HOMO} than PTB7-Th led to an increased V_{OC} of 0.90 V and a PCE of 11.2%, and thereby a decreased E_{loss} of 0.70 eV.¹⁰⁸

Derivatives of ITIC were synthesized by introducing substituents on the 3-DCM end-capping groups. Hou and co-workers synthesized fluorinated and chlorinated derivatives IT-4F¹⁶ and IT-4Cl (**Figure 8**),¹⁰⁹ respectively, which had downshifted energy levels relative to ITIC owing to the electron-withdrawing nature of the fluorine and chlorine atoms, and had slightly reduced E_g values of 1.55 and 1.48 eV, respectively. IT-4F was combined with PBDB-TSF, which also had downshifted energy levels relative to PBDB-T. The PBDB-TSF/IT-4F cell showed a V_{OC} of 0.88 V and thus an E_{loss} of 0.66 eV, which was similar to that for the PBDB-T/ITIC cell, but gave a high EQE_{max} of 83% and a high PCE of 13.0%.¹⁶ IT-4Cl was combined with PBDB-TF, which is also called PM6, and the cell exhibited a V_{OC} of 0.79 V, which resulted in an E_{loss} of 0.69 eV, and a PCE as high as 13.5%.¹⁰⁹ The same group also reported IT-M and IT-DM (**Figure 8**), in which one methyl group and two methyl groups were introduced on the DCM moiety, respectively. IT-M and IT-DM had upshifted energy levels, in particular E_{LUMO} , relative to ITIC due to the electron-donating nature of the methyl group, whereas they had slightly wide E_g s.¹¹⁰ When PBDB-T was used as the p-type polymer, the IT-M and IT-DM cells showed increased V_{OC} values of 0.94 and 0.97 V, respectively, both resulting in the same small E_{loss} of 0.66 eV.

Chen and colleagues investigated a series of NFAs with a CDT-flanked difluorophenyl moiety as the central core, namely, DF-PCIC, HC-PCIC, and FO-PCIC (**Figure 8**), which had deep E_{HOMO} s of around -5.5 eV. They prepared six polymer/NFA blends using three different polymers, such as PBDB-T, PBDB-TF, and PTQ-10 (**Figure 9**), and these NFAs, with ΔE_{H} values varying from -0.05 to 0.21 eV.¹¹¹ Interestingly, despite the fact that the PTQ10/HC-PCIC and PBDB-TF/HC-PCIC cells had ΔE_{H} values of nearly zero and 0.06 eV, respectively, those cells afforded quite high EQE_{max} s of around 70%, leading to high PCEs of 10.4 and 11.8%, respectively. Further, the E_{loss} values for the PTQ10/HC-PCIC and PBDB-TF/HC-PCIC cells were found to be 0.55 and 0.59 eV, respectively.

With the alkoxythiophene groups attached between the IDT core and the DCM end-capping group, IEICO had a shallow E_{HOMO} relative to ITIC but a similar E_{LUMO} and a very small E_{g} of 1.34 eV.¹¹² When IEICO was combined with PBDTTT-E-T in which the fluorine atom in PTB7-Th was replaced with the hydrogen atom, the ΔE_{H} was as small as 0.23 eV. The PBDTTT-E-T/IEICO cell showed a maximum PCE of 8.4% along with a relatively high V_{OC} of 0.82 eV, giving rise to a small E_{loss} of 0.52 eV. Similarly to the ITIC system, the fluorinated and chlorinated versions of IEICO, named IEICO-4F¹¹³ and IEICO-4Cl,¹¹⁴ were also reported (**Figure 8**). IEICO-4F and IEICO-4Cl showed slightly reduced E_{g} s of 1.24 and 1.23 eV, and deep energy levels relative to IEICO, respectively. IEICO-4F and IEICO-4Cl were combined with PTB7-Th, where the ΔE_{H} values were 0.20 eV for PTB7-Th/IEICO-4F and 0.32 eV for PTB7-Th/IEICO-4Cl blends. As a result, the PTB7-Th/IEICO-4F and PTB7-Th/IEICO-4Cl cells exhibited V_{OC} values of 0.74 and 0.73 V, respectively, and consequently very small E_{loss} s of 0.50 eV. Due to the relatively high EQE_{max} of around 70%, the cell had high J_{SCS} of more than 20 mA cm⁻² and PCEs of around 10.0% for both cells. Although the reason is yet unclear, the cells based on these IEICO series showed even smaller E_{loss} s than the cells based on PCIC series as described above despite the larger ΔE_{H} values. This might be due to the determination of E_{g} as well as ΔE_{H} or possibly the difference in other loss factors.

ITIC-like NFAs having different central cores with small E_{g} s were also investigated. Chen and co-workers designed 6TIC¹¹⁵ and 3TT-FIC (**Figure 8**),¹¹⁶ in which three thieno[3,2-*b*]thiophene units bridged by a carbon atom were employed as the central core along with the DCM end-capping groups. 6TIC and 3TT-FIC showed broad and strong absorptions, exhibiting onset absorption wavelengths of 905 and 995 nm, which corresponded to E_{g} s of 1.37 and 1.25 eV, respectively. The E_{HOMO} values for these materials were around -5.4 eV, resulting in the ΔE_{H} values of 0.21 and 0.18 eV for 6TIC and 3TT-FIC cells, respectively, when blended with PTB7-Th, respectively. The PTB7-Th/6TIC cell exhibited a V_{OC} of 0.83 V and thus a relatively small E_{loss} of 0.54 eV, along with a PCE of 10.7%, whereas the PTB7-Th/3TT-FIC cell showed a V_{OC} of 0.66 V and thus a slightly larger E_{loss} of 0.59 eV, but with a higher PCE of 12.2%.

Ding and co-workers reported a narrow-bandgap NFA, CO*i*8DFIC (**Figure 8**),^{117,118,119} in which the central fused-ring core has three thieno[3,2-*b*]thiophene units similar to 3TT-FIC, but these thienothiophenes are bridged by a C–O bond, forming 2*H*-pyran groups. CO*i*8DFIC was reported to have an E_g of 1.18 eV and an E_{HOMO} of -5.50 eV. Among NFAs with the CO-bridged ladder-type central cores,¹²⁰ CO*i*8DFIC had the narrowest E_g . When PTB7-Th was combined, the ΔE_{H} was found to be about 0.25 eV. The PTB7-Th/CO*i*8DFIC cell showed a V_{OC} of 0.68 V and thus a small E_{loss} of 0.50 eV, along with 12.2% PCE.¹²¹ In addition, a PTB7-Th/CO*i*8DFIC/PC₇₁BM ternary cell exhibited an improved V_{OC} of 0.73 V, perhaps being affected by the relatively shallow E_{LUMO} for PC₇₁BM, which led to a significantly small E_{loss} of 0.45 eV, but a significantly high EQE_{max} of 85% and a high PCE of 14.6%.¹¹⁷

Jen and co-workers reported NFAs that were based on a highly π -extended electron-rich dithienopicenocarbazole moiety as the central core, DTPC-IC and DTPC-DFIC (**Figure 8**).¹²² DTPC-IC and DTPC-DFIC had very narrow E_g s of 1.24 and 1.21 eV, and E_{HOMOS} of -5.21 and -5.31 eV, resulting in very small ΔE_{H} values of 0.01 and 0.11 eV, respectively, when combined with PTB7-Th. Although the PTB7-Th/DTPC-IC cell showed poor performance with a PCE of 3.1% because of the low EQE_{max} of 28%, a high V_{OC} of 0.86 V for such a narrow-bandgap system was observed, resulting in an extremely small E_{loss} of 0.42 eV. In contrast, the PTB7-Th/DTPC-DFIC cell showed a high PCE of 10.2% owing to the significantly enhanced EQE_{max} of 69% compared to the DTPC-IC cell even though the E_{loss} was still significantly small at 0.45 eV.

Li and co-workers employed a highly π -extended electron-deficient dithienothienopyrrolobenzothiadiazole (TPBT) as the central core of DCM-end-capped NFAs, namely, Y5¹²³ and Y6 (**Figure 8**).¹⁷ Y5 and Y6 exhibited relatively broad and strong absorptions, showing onset absorption wavelengths of 900 and 931 nm, which corresponded to the E_g s of 1.38 and 1.33 eV, along with relatively deep E_{HOMOS} of -5.55 and -5.65 eV, respectively. Thus, the ΔE_{H} values of PBDB-T/Y5 and PBDB-TF/Y6 blends were found to be 0.22 and 0.20 eV, respectively. The PBDB-T/Y5 cell exhibited a V_{OC} of 0.88 V, thus an E_{loss} of 0.50 eV, and a high EQE_{max} of 75%,

which resulted in a high PCE of 14.1%. The PBDB-TF/Y6 cell exhibited a similar E_{loss} of 0.50 eV with a V_{OC} of 0.83 V, but gave an even higher EQE_{max} of 83% and an improved PCE of 15.7%. Further, a similar NFA in which fluorine atoms on the DCM moieties were replaced with chlorine atoms, named BTP-4Cl or Y7 (**Figure 8**), was reported.¹²⁴ BTP-4Cl had a similar E_{g} of 1.40 eV and slightly downshifted energy levels ($E_{\text{HOMO}} = -5.68$ eV, $E_{\text{LUMO}} = -4.12$ eV) relative to Y6. Note that in this report, the E_{g} s for Y6 and BTP-4Cl were determined from the intersection of the absorption and fluorescence spectra, thereby the E_{g} for Y6 differed from that in the earlier report.¹⁷ The PBDB-TF/BTP-4Cl cell showed a slightly improved V_{OC} of 0.87 V, resulting in a small E_{loss} of 0.53 eV, along with a high PCE of 16.5% relative to the PBDB-TF/Y6 cell. Interestingly, although BTP-4Cl showed a deeper E_{LUMO} than its fluorinated analog Y6, the BTP-4Cl cell exhibited higher V_{OC} than the Y6 cell even when the same p-type polymer was combined. This originated in its reduced energy loss by non-radiative recombination ($q\Delta V_{\text{nr}}$).

Interestingly, the group of Hou, He, and Meng designed an NFA molecule,¹²⁵ ANT-4F (**Figure 8**), by replacing the IDTT core of IT-4F with anthracene, which is a strongly fluorescent chromophore compared with thiophene-based ones. They expected that the incorporation of a more fluorescent chromophore would lead to higher quantum efficiency even from the CT exciton of the blend system, which would result in a reduced $q\Delta V_{\text{nr}}$. In fact, ANT-4F showed significantly higher PL intensity than IT-4F in the neat film. Further, the PBDB-TF/ANT-4F blend film exhibited higher efficiency in the EL measurement as well as in the PL measurement. As a result, $q\Delta V_{\text{nr}}$ for the ANT-4F cell was found to be 0.22 eV, which was 0.06 eV smaller than that for the IT-4F cell. Although the overall E_{loss} was 0.74 eV for the ANT-4F cell and 0.79 eV for the IT-4F cell, which was not significantly small, the main difference in E_{loss} originated in the difference in $q\Delta V_{\text{nr}}$. Hou and co-workers reported a series of TPBT-based molecules in which the number of the fluorine atom on the DCM group was 0, 2, 4, and 6 (BTP-0F, BTP-2F, BTP-4F, and BTP-6F), respectively, (**Figure 8**).¹²⁶ They found that the intermolecular interactions between these molecules and PBDB-TF polymer were enhanced by increasing the fluorine number. This facilitated the charge generation and in turn improved the J_{SC} .

On the other hand, the intermolecular interactions were decreased by decreasing the fluorine number, which resulted in the enhanced hybridization of LE and CT states. This led to the higher EQE_{EL} and thus the smaller $q\Delta V_{\text{nr}}$: $q\Delta V_{\text{nr}}$ was 0.23, 0.22, 0.19, and 0.15 eV for the BTP-6F, BTP-4F, BTP-2F, and BTP-0F cells, respectively. Unfortunately, the BTP-0F cell with the smallest $q\Delta V_{\text{nr}}$ showed the lowest PCE of 8.2% among these cells due to the low EQE. The highest PCE was observed for the BTP-4F (PCE = 16.7%, $q\Delta V_{\text{nr}} = 0.22$ eV) cell due to the balanced J_{SC} , V_{OC} , and FF. In addition, Y11 having the benzotriazole moiety instead of the benzothiadiazole moiety for Y6 showed a smaller $q\Delta V_{\text{nr}}$ of 0.20 eV with a PCE of 16.5% when blended with PBDB-TF ($q\Delta V_{\text{nr}}$ was reported to be as small as 0.17 eV when the PCE was 13.8%), likely due to the negligible ΔE and the low energetic disorder evidenced by a very small E_{U} of 26 meV.²²

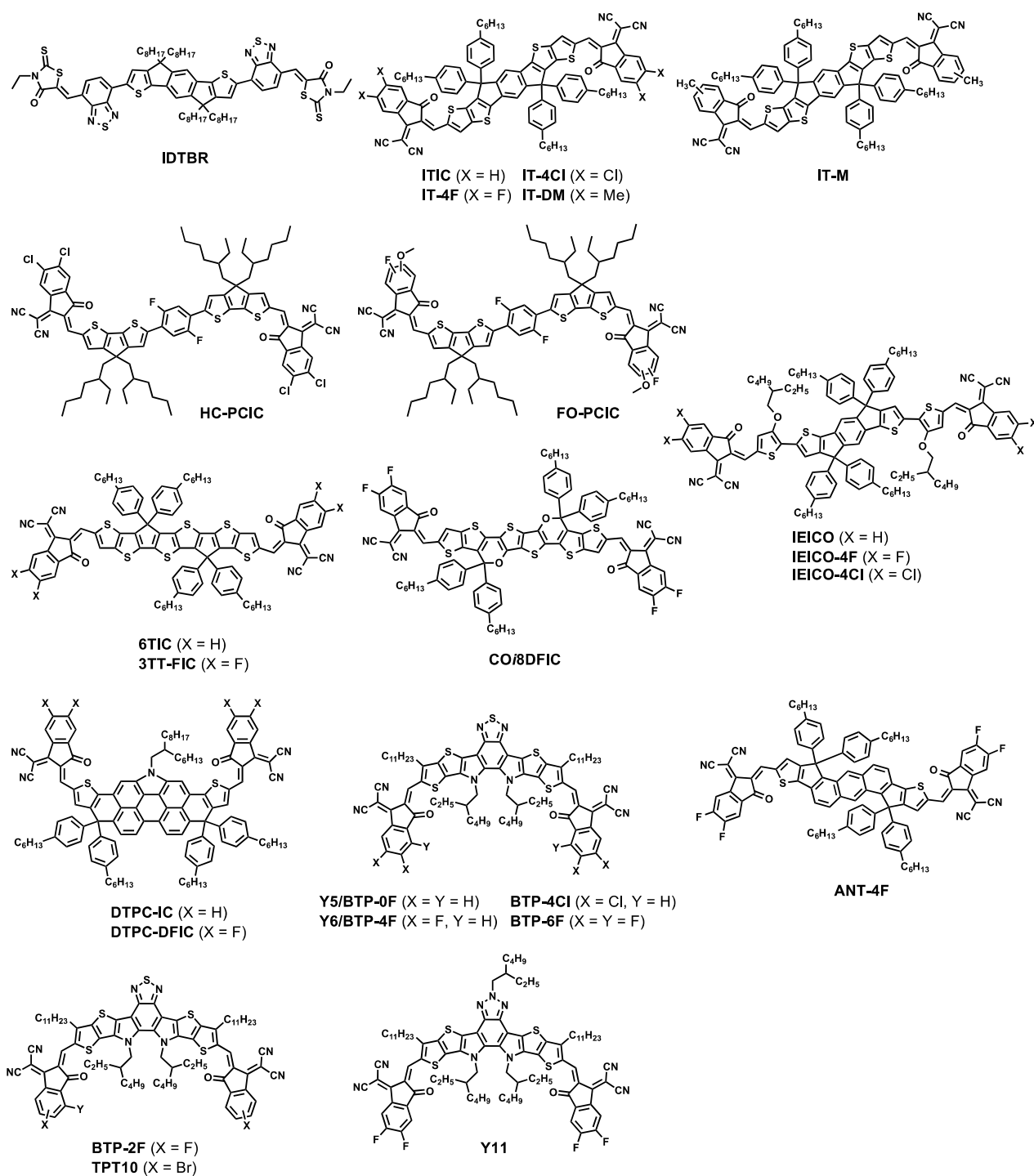


Figure 8. (a) Narrow-bandgap non-fullerene acceptors. (b) p-Type π -conjugated polymers combined with these non-fullerene acceptors.

Table 4. Electronic and photovoltaic properties of narrow-bandgap non-fullerene acceptors

Narrow-bandgap NFA	E_g (eV) ^a	$E_{\text{HOMO}}/$ E_{LUMO} (eV) ^b	p-type polymer/ E_g (eV) ^c	ΔE_{H} (eV)	EQE_{max} (%)	J_{SC} (mA cm^{-2})	V_{OC} (V)	FF	PCE_{max} (%)	E_{loss} (eV)	ref
IDTBR	1.63	−5.45/ −3.90	PffBT4T- DT	0.16	76	15.0	1.07	0.62	9.9	0.56	106
			PffBT2T- TT/ 1.63	0.09	67	14.3	1.08	0.67	10.4	0.55	107
ITIC	1.60	−5.61/ −4.02	PTB7-Th /1.58	0.37	73	14.2	0.81	0.59	6.3	0.79	14
			PBDB-T/ 1.82	0.18	75 ^c	16.8	0.90	0.74	11.2	0.70	108
IT-4F	1.55	−5.66/ −4.14	PBDB- TSF/ 1.80	0.26	83	20.5	0.88	0.72	13.0	0.66	16
IT-4Cl	1.48	−5.75/ −4.27	PBDB-TF (PM6)/ 1.80	0.30	80	22.7	0.79	0.75	13.5	0.69	109
IT-M	1.60	−5.58/ −3.98	PBDB-T/ 1.82	0.25	78 ^c	17.4	0.94	0.74	12.1	0.66	110
IT-DM	1.63	−5.56/ −3.93	PBDB-T/ 1.82	0.23	76 ^c	16.5	0.97	0.71	11.3	0.66	110
HC-PCIC	1.48	−5.54/ −3.87	PTQ10/ 1.92	0.00	68 ^c	16.0	0.94	0.68	10.4	0.55	111
			PBDB-TF/ 1.80	0.06	78	18.1	0.89	0.72	11.8	0.59	111
IEICO	1.34	−5.32/ −3.95	PBDTTT- E-T/ 1.59	0.23	68	17.7	0.82	0.58	8.4	0.52	112
IEICO-4F	1.24	−5.44/ −4.19	PTB7-Th/ 1.58	0.20	74 ^c	22.8	0.74	0.59	10.0	0.50	113
IEICO-4Cl	1.23	−5.56/ −4.23	PTB7-Th/ 1.58	0.32	72 ^c	22.8	0.73	0.62	10.3	0.50	114
6TIC	1.37	−5.45/ −3.94	PTB7-Th/ 1.58	0.22	78 ^c	19.6	0.83	0.66	10.7	0.54	115
3TT-FIC	1.25	−5.42/ −4.17	PTB7-Th/ 1.58	0.18	81 ^c	25.9	0.66	0.71	12.2	0.59	116
CO ₈ DFIC	1.18	−5.50/ −3.88	PTB7-Th/ 1.58	0.11	75 ^c	26.1	0.68	0.68	12.2	0.50	118
CO ₈ DFIC (ternary with PCBM)			PTB7-Th/ 1.58	0.11	85 ^c	27.4	0.73	0.73	14.6	0.45	117
DTPC-IC	1.28	−5.21/ −3.97	PTB7-Th/ 1.58	0.01	28 ^c	8.5	0.86	0.42	3.1	0.42	122
DTPC-DFIC	1.21	−5.31/ −4.10	PTB7-Th/ 1.58	0.11	69	21.9	0.76	0.61	10.2	0.45	122
Y5 (BTP-0F)	1.38	−5.55/ −3.88	PBDB-T/ 1.82	0.17	75 ^c	22.8	0.88	0.70	14.1	0.50	123

		-3.87	1.82								
	-	-5.59/ -3.79	PBDB-TF/ 1.80	0.14	48 ^e	15.2	0.96	0.57	8.2	~-0.51	126
BTP-2F	-	-5.64/ -3.85	PBDB-TF/ 1.80	0.19	76 ^e	22.1	0.89	0.72	14.1	~-0.54	126
Y6 (BTP-4F)	1.33	-5.65/ -4.10	PBDB-TF/ 1.80	0.09	83 ^e	25.3	0.83	0.75	15.7	0.50	17
	1.40 ^d	-5.65/ -4.02	PBDB-TF/ 1.80	0.20	85	24.9	0.83	0.75	15.6	0.57	124
	-	-5.68/ -3.89	PBDB-TF/ 1.80	0.23	81 ^e	25.3	0.85	0.78	16.7	~-0.55	126
BTP-6F	-	-5.69/ -3.97	PBDB-TF/ 1.80	0.24	82 ^e	25.9	0.81	0.73	15.3	~-0.57	126
BTP-4Cl	1.40 ^d	-5.68/ -4.12	PBDB-TF/ 1.80	0.23	85	25.4	0.87	0.75	16.5	0.53	124
Y11	1.31	-5.69/ -3.87	PBDB-TF/ 1.80	0.17	79	26.6	0.85	0.75	16.5	0.46	22
ANT-4F	1.67	-5.69/ -4.01	PBDB-TF/ 1.80	0.15	78	19.0	0.93	0.74	13.1	0.74	125

a) Optical bandgap determined from the absorption onset. b) HOMO and LUMO energy levels determined by CV. c) p-type semiconducting polymer combined in the photovoltaic cell/optical bandgap of the polymer. d) E_g determined from the intersection of the absorption and fluorescence spectra. e) maximum EQE value extracted from the EQE spectrum in the corresponding literature by the authors of this review.

5-2. Wide-bandgap p-type polymers

The variety of wide-bandgap p-type polymers for efficient polymer/NFA cells is somewhat limited. Most of them consist of an electron-rich BDT fused-ring unit having a thiophene-based side chain and a weak electron-deficient heteroaromatic unit. Specifically, a series of PBDB-T polymers (**Figure 9**), namely, BDT-benzo[1,2-*c*:4,5-*c'*]dithiophene-4,8-dione polymers, are often used. Hou and co-workers demonstrated that the PBDB-T/ITIC cell exhibited as high as 11.2% PCE whereas the PBDB-T/PC₇₁BM cell showed a PCE of 7.5%, thereby providing the first example of the PCE of NFA-based cells being higher than that of fullerene-based cells.^{108,127} Thereafter, fluorinated, thioalkylated, and chlorinated PBDB-T polymers, namely, PBDB-TF (PM6),^{128,129} PBDB-TSF,¹⁶ and PBDB-T-2Cl,¹³⁰ respectively, were synthesized and investigated. All these polymers had deeper E_{HOMOS} than PBDB-T and thus had smaller ΔE_{H} values: for example, ΔE_{H} was more than 0.3 eV for PBDB-T whereas it was 0.19 eV for PBDB-TF, 0.26 eV for PBDB-TSF, and 0.15 eV for PBDB-T-2Cl, with respect to IT-4F. The PCE was improved to 13.2% for PBDB-TF, 13.0% for PBDB-TSF, and 14.4% for PBDB-T-2Cl relative to that for PBDB-T (10.1%). The E_{loss} values for these cells were around 0.7 eV, which were similar to that for the PBDB-T/ITIC cell.

Peng and colleagues reported PBDT-TDZ and PBDTS-TDZ (**Figure 9**),¹³¹ which incorporate BDT and 1,3,4-triazole as the fused ring building units. These copolymers exhibited the same E_{g} of 2.07 eV and E_{HOMOS} of -5.35 and -5.39 eV, respectively, which led to small ΔE_{HS} of ~ 0.13 eV. Their blend systems exhibited good complementary absorption covering the entire visible range of 300 to 800 nm. Whereas the PBDT-TDZ/ITIC cell exhibited a V_{OC} of 1.01 V and an E_{loss} of 0.56 eV, the PBDTS-TDZ/ITIC cell exhibited a high V_{OC} of 1.10 V and an extremely small E_{loss} of 0.47 eV. Moreover, the PBDTS-TDZ/ITIC cell gave a high EQE_{max} of 79%, which was similar to the PBDT-TDS/ITIC cell, and a high PCE of 12.8% despite the fact that the E_{loss} was extremely small. The same group also synthesized copolymer PBDT-ODZ based on 1,3,4-oxadiazole (**Figure 9**).¹³² With the E_{HOMO} of -5.68 eV, PBDT-ODZ had a ΔE_{H} of 0.1 eV when paired with ITIC-Th. The PBDT-

ODZ/ITIC-Th cell exhibited a high V_{OC} of 1.08 V, which resulted in a small E_{loss} of 0.50 eV, but gave a high EQE_{max} of 75% and a high PCE of 10.1%.

Ding and co-workers reported several BDT-based polymers with different fused-rings as the co-building unit, such as 5*H*-dithieno[3,2-*b*:2',3'-*d*]pyran-5-one (L1 and L2),¹³³ 5*H*-dithieno[3,2-*b*:2',3'-*d*]thiopyran-5-one (D16),¹³⁴ and dithieno[3',2':3,4;2'',3''':5,6]benzo[1,2-*c*][1,2,5]thiadiazole (D18)²⁰ (**Figure 9**). L1 and L2 were reported to have E_{HOMO} s of -5.45 and -5.52 eV, resulting in the ΔE_H values of 0.20 and 0.13 eV, respectively, when blended with Y6. The V_{OC} was higher for the L2 cell (0.87 V) than the L1 cell (0.80 V), and thus the E_{loss} was smaller for the L2 cell (0.46 eV) than the L1 cell (0.53 eV). However, the PCE was higher for the L1 cell (14.4%) than the L2 cell (12.6%), owing to the higher EQE_{max} for the L1 cell (79%) than in the L2 cell (68%), which seems to be as a result of larger ΔE_H for the L1 cell. The E_{HOMO} s of D16 and D18 were -5.48 and -5.51 eV, and hence ΔE_H s for the D16/Y6 and D18/Y6 blends were 0.17 and 0.14 eV, respectively. The D16 and D18 cells provided V_{OC} s of 0.83 and 0.86 V, resulting in E_{loss} s of 0.50 and 0.47 V, respectively. These cells showed very high EQE_{max} of around 85%. Whereas the D16 cell exhibited a PCE of 16.0%, the D18 cell exhibited a significantly high PCE of 18.2%.

Apart from BDT-based polymers, Li and co-workers reported a quinoxaline-based polymer, PTQ10 (**Figure 9**),¹³⁵ which was synthesized through a two-step reaction using inexpensive raw materials. The E_{HOMO} and E_g values for PTQ10 were reported to be -5.54 and 1.92 eV, respectively. Thus, when IDIC having an E_{HOMO} of -5.74 eV and an E_g of 1.57 eV was combined, ΔE_H was found to be 0.20 eV. The PTQ10/IDIC cell exhibited a V_{OC} of 0.97 V, giving rise to an E_{loss} of 0.60 eV, and a PCE as high as 12.7%. The same group also reported a derivative of PTQ10, PTQ11, in which the methyl group was introduced in the quinoxaline unit (**Figure 9**).¹³⁶ PTQ11 was combined with TPT10 (**Figure 8**), having the bromine atom instead of the fluorine atom of BTP-2F, which showed efficient hole transfer from TPT10 to PTQ11 despite the negligible ΔE_H . The PTQ11/TPT10 cell still exhibited a very high EQE_{max} of 86%. As a result, the PTQ11/TPT10 cell gave a PCE of 16.3% with an E_{loss} of 0.48 eV. Yan and co-workers reported the wide-bandgap polymer PvBDTTAZ (**Figure 9**) having an

E_g of 2.05 eV, which incorporated an unsubstituted BDT unit and a weak electron-deficient benzotriazole unit. In this polymer, the unsubstituted BDT unit was linked to the phenyl position unlike other BDT-based polymers, which would give rise to a twisted backbone due to the steric hindrance at the peri-positions. PvBDTTAZ had an E_{HOMO} of -5.47 eV, and thereby ΔE_{H} was 0.20 eV when blended with IDTBR. The PvBDTTAZ/IDTBR cell exhibited a high V_{OC} of 1.08 V, leading to a small E_{loss} of 0.55 eV, and a relatively high PCE of 11.6%.¹³⁷

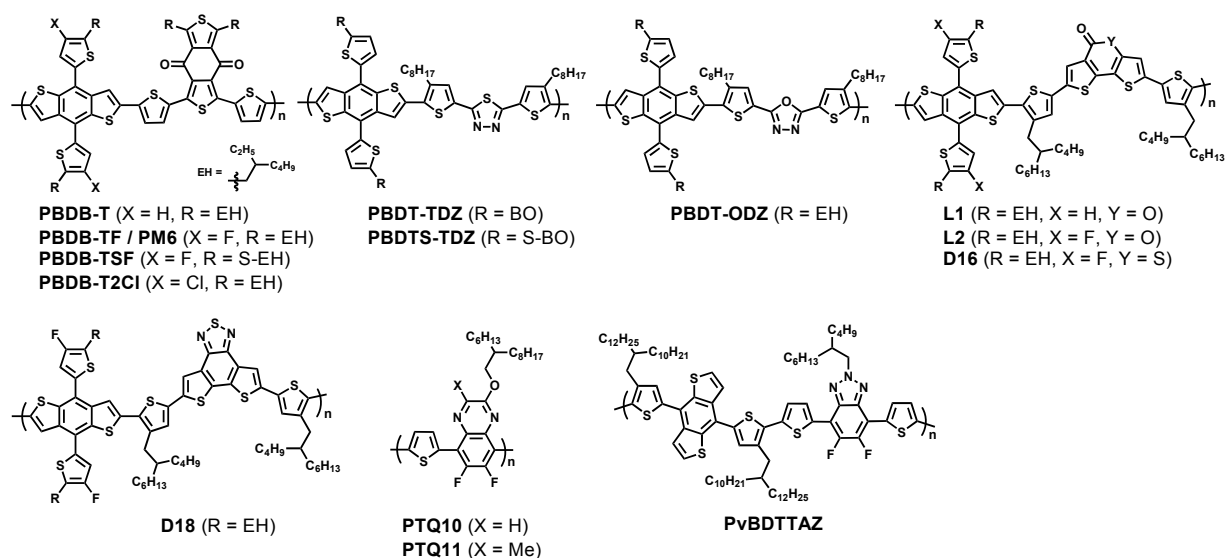


Figure 9. Wide-bandgap p-type polymers typically combined with narrow-bandgap non-fullerenes.

Table 5. Electronic and photovoltaic properties of wide-bandgap p-type polymers used for NFA-based photovoltaic cells

Wide-bandgap p-type polymer	E_g (eV) ^a	$E_{\text{HOMO}}/ E_{\text{LUMO}}$ (eV) ^b	NFA/ E_g (eV) ^c	ΔE_{H} (eV)	EQE_{max} (%)	J_{SC} (mA cm ⁻²)	V_{OC} (V)	FF	PCE_{max} (%)	E_{loss} (eV)	ref
PBDB-T	1.82	-5.33/ -2.92	ITIC/1.57	0.18	75 ^d	16.8	0.90	0.74	11.2	0.67	108
			IT-4F/1.55	0.45	76 ^d	19.6	0.72	0.71	10.1	0.83	138
PBDB-TF	1.80	-5.45/ -3.65	IT-4F/1.55	0.25	78 ^d	20.8	0.84	0.76	13.2	0.71	130
PBDB-TSF	1.80	-5.40/ -3.60	IT-4F/1.55	0.26	83	20.5	0.88	0.72	13.0	0.66	16
PBDB-T2Cl	1.80	-5.51/ NA	IT-4F/1.55	0.19	82 ^d	21.8	0.86	0.77	14.4	0.69	130
PBDT-TDZ	2.07	-5.35/ -2.78	ITIC/1.57	0.13	77 ^d	17.2	1.01	0.68	11.7	0.56	131
PBDTS-TDZ	2.07	-5.39/ -2.80	ITIC/1.57	0.09	79 ^d	17.8	1.10	0.65	12.8	0.47	131
PBDT-ODZ	2.12	-5.68/ -2.89	ITIC- Th/1.57	0.10	75 ^d	15.5	1.08	0.60	10.1	0.50	132
L1	1.96	-5.45/ -2.79	Y6/1.33	0.20	79	23.9	0.80	0.75	14.4	0.53	133
L2	1.96	-5.52/ -2.91	Y6/1.33	0.13	68	20.5	0.87	0.70	12.6	0.46	133
D16	1.95	-5.48/ -2.83	Y6/1.33	0.17	83 ^d	25.7	0.83	0.75	16.0	0.50	134
D18	1.98	-5.51/ -2.77	Y6/1.33	0.14	86 ^d	27.7	0.86	0.77	18.2	0.47	20
PTQ10	1.92	-5.54/ -2.98	IDIC/1.57	0.20	78 ^d	17.8	0.97	0.74	12.7	0.60	135
PTQ11	1.95	-5.52/ -2.76	TPT10/1.36	0.00	86 ^d	24.8	0.88	0.75	16.3	0.48	136
PvBDTTAZ	2.05	-5.47/ -3.42	IDTBR/1.63	0.04	71 ^d	16.3	1.08	0.64	11.6	0.55	137

a) Optical bandgap determined from the absorption onset. b) HOMO and LUMO energy levels determined by CV. c) NFA combined in the photovoltaic cell/optical bandgap of the NFA material. d) maximum EQE value extracted from the EQE spectrum in the corresponding literature by the authors of this review.

5-3. Summary

Wide and narrow bandgap NFAs, along with wide-bandgap p-type polymers that are employed as a pair to a narrow-bandgap NFA were summarized. In the wide-bandgap NFAs, most of the materials consist of PDI or PDI derivatives, which are long-known organic dye moieties with relatively strong electron deficiency. Further, the PDI moieties are linked to a core building unit in a highly twisted manner, avoiding aggregation. These wide-bandgap NFAs are generally combined with narrow-bandgap p-type polymers. In particular, difluorobenzothiadiazole-based polymers are mostly employed. As the ΔE_L is a crucial factor for reducing the E_{loss} in such cases, these NFAs have relatively shallow E_{LUMOS} .

With respect to the narrow-bandgap NFAs, they consist of rigid rod π -conjugated cores, many of which are highly π -extended ladder-type fused heteroaromatics, which are end-capped with electron-deficient functional groups, such as rhodamine or DCMs. These materials typically have deep E_{HOMOS} , which are similar to that for the combined wide-bandgap polymer. The E_{HOMO} is markedly affected by the core unit, whereas the E_{LUMO} of the narrow-bandgap NFAs is strongly affected by the end-capping group. In order to tune the energy levels, various fused-ring π -conjugated systems are incorporated as the core moiety, whereas such halogens as fluorine and chlorine atoms and methyl groups are typically substituted in the DCM end-capping groups.

It is also noted that some reports have shown that ΔV_{nr} can be reduced by tuning the molecular structure. In both wide- and narrow-bandgap NFAs, a small E_{loss} of around 0.5 eV has been reported. This is again probably because of LE–CT hybridization as is the case in some narrow-bandgap polymer/PCBM systems. Note that the wide-bandgap polymer/narrow-bandgap NFA systems tended to afford higher EQEs and thereby higher PCEs under small E_{loss} s than narrow-bandgap polymer/wide-bandgap NFA systems as well as narrow-bandgap polymer/PCBM systems. Whereas the cells that use the wide-bandgap NFAs have been shown to give moderately high PCEs of 5–10%, the cells that use the narrow-bandgap NFAs have demonstrated significantly high PCEs of up to 18%. This is partly because narrow-bandgap NFAs are likely to exhibit higher EQE even at the near-IR

region than typical narrow-bandgap polymers, and partly because narrow-bandgap NFAs are likely to exhibit smaller $q\Delta V_r$ owing to smaller E_U , which is similar to narrow-bandgap polymers as mentioned before.

6. Polymer/polymer cells (All-polymer cells)

Organic solar cells that employ π -conjugated polymers for both p-type and n-type semiconductors, called all-polymer solar cells, are thought to have advantages in blend morphology stability and thus device stability over polymer/small-molecule and all-small-molecule solar cells.^{139,140} Although the performance of all-polymer cells has lagged far behind that of polymer/fullerene cells, recent effort in materials development, specifically n-type polymers, has resulted in small E_{loss} and boosted the performance with PCEs that are as high as 11%.^{140,141} In this section, we summarize wide- and narrow-bandgap n-type polymers that enable small E_{loss} in all-polymer solar cells (**Figures 10** and **11**). The electronic and solar cell properties for wide- and narrow-bandgap n-type polymers are summarized in **Tables 6** and **7**, respectively.

6-1. Wide-bandgap n-type polymers

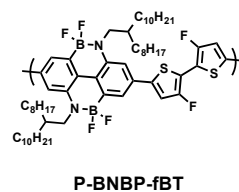
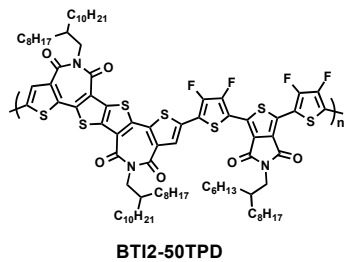
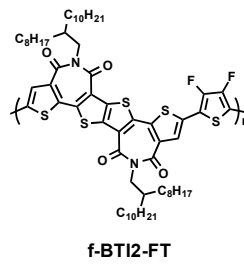
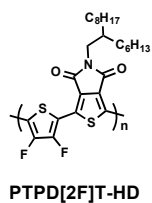
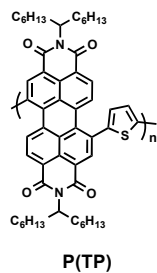
PDI had often been used as the building unit of n-type polymers in early studies.¹⁴² Bao and co-workers employed a polymer, P(TP) (**Figure 10**), consisting of PDI and thiophene, which was combined with a series of isoindigo-based p-type polymers.¹⁴³ When P(TP) was blended with the isoindigo-bithiophene polymer PiI-2T in which 5% of the side chain was polystyrene instead of a common branched alkyl group, the ΔE_{L} was found to be as small as 0.1 eV. The solar cell composed of PiI-2T and P(TP) showed a high V_{OC} of 1.04 V and thereby a small E_{loss} of 0.61 eV, although it gave a modest PCE of 4.4%.

Beaujuge and co-workers reported an all-polymer cell that used an n-type polymer consisting of thienopyrrole-dione and difluorothiophene, PTPD[2F]T (**Figure 10**), having an E_{g} of approximately 1.9 eV and an E_{LUMO} of -3.8 eV.¹⁴⁴ When PTPD[2F]T was combined with PTB7-Th that possesses an E_{g} of 1.58 eV, although ΔE_{L} was approximately 0.3 eV according to the reported E_{LUMO} , the cell showed a V_{OC} that was as high as 1.1 V, which resulted in an E_{loss} of approximately 0.5 eV, with a modest PCE of 4.4%.

As shown above, imide-functionalized heteroaromatics are important building units for n-type polymers.¹⁴⁵ Imide-functionalized units that specifically afford wide-bandgap n-type polymers also include bithiopheneimide (BTI)^{146,147} and dithienothiophenebisimide (TBI or f-BTI2).^{148,149} Guo and co-workers reported a polymer consisting of f-BTI2 and difluorothiophene, named f-BTI2-FT (**Figure 10**), having an E_g of 1.84 eV and an E_{LUMO} of -3.43 eV.¹⁵⁰ Although the ΔE_L was relatively large at 0.40 eV, the PTB7-Th/f-BTI2-FT cell showed as high as 1.04 V V_{OC} , resulting in the E_{loss} of as small as 0.54 eV, with a PCE of 6.9%. The same group also reported random copolymers based on f-BTI2, difluorothiophene, and thienopyrrole-dione, BTI2- x TPD, where $x = 0.1, 0.3,$ and 0.5 (**Figure 10**).¹⁵¹ All the polymers had E_g s of around 1.87 eV and E_{LUMOS} of around -3.40 eV, which were similar to those of f-BTI2-FT. When x was 0.5 (BTI2-50TPD), the cell that used PTB7-Th as the p-type polymer gave the highest V_{OC} of 1.05 V among these polymers, which resulted in a small E_{loss} of 0.53 eV. The EQE_{max} in the absorption range for BTI2-50TPD was approximately 60%, which should be fairly high for small- E_{loss} cell, leading to a relatively high PCE of 8.3%.

A copolymer based on bipyridine in which two pyridine moieties are bridged with a boron–nitrogen coordination bond, P-BNBP-fBT (**Figure 10**), was also reported to show a small E_{loss} when blended with PTB7-Th.¹⁵² P-BNBP-fBT had an E_g and an E_{LUMO} of 1.86 and -3.62 eV, respectively, and thus the ΔE_L was found to be 0.18 eV. The PTB7-Th/P-BNBP-fBT cell exhibited a PCE of 6.3% with a high V_{OC} of 1.07 V, and thereby an E_{loss} of as small as 0.51 eV.

(a)



(b)

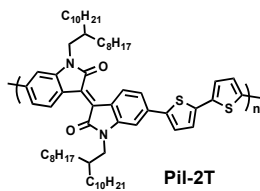


Figure 10. Wide-bandgap n-type polymers.

Table 6. Electronic and photovoltaic properties of wide-bandgap n-type polymers

Wide-bandgap n-type polymer	E_g (eV) ^a	$E_{\text{HOMO}}/E_{\text{LUMO}}$ (eV) ^b	p-type/ E_g (eV) ^c	ΔE_L (eV)	EQE_{max} (%)	J_{SC} (mA cm ⁻²)	V_{OC} (V)	FF	PCE_{max} (%)	E_{loss} (eV)	ref
P(TP)	1.80	-5.60/ -3.80	PiI-2T/ 1.65	0.04	37 ^d	9.0	1.04	0.47	4.4	0.61	143
PTPD[2F]T-HD	1.90	-5.91/ -4.04	PTB7- Th/ 1.58	0.61	50	8.4	1.10	0.44	4.4	0.51	144
f-BTI2-FT	1.84	-5.27/ -3.43	PTB7- Th/ 1.58	0.40	57 ^d	11.6	1.04	0.57	6.9	0.54	150
BTI2-50TPD	1.87	-6.16/ -3.40	PTB7- Th/ 1.58	0.08	68 ^d	13.6	1.05	0.58	8.3	0.53	151
P-BNBP-fBT	1.86	-5.87/ -3.62	PTB7- Th/ 1.58	0.18	58 ^d	12.7	1.07	0.47	6.3	0.51	152

a) Optical bandgap determined from the absorption onset. b) HOMO and LUMO energy levels determined by CV. c) p-type semiconducting polymer combined in the photovoltaic cell/optical bandgap of the polymer. d) maximum EQE value extracted from the EQE spectrum in the corresponding literature by the authors of this review.

6-2. Narrow-bandgap n-type polymers

Most of the n-type polymers with narrow bandgaps are based on naphthalenediimide (NDI).¹⁴⁵ Since early studies of all-polymer solar cells, copolymers consisting of NDI and bithiophene, named P(NDI2OD-2T) or N2200 (**Figure 11a**),^{153,154} have been the common n-type polymers. The E_g , E_{HOMO} , and E_{LUMO} for N2200 were reported to be typically around 1.45 eV, -5.4 to -5.5 eV, and -3.8 to -3.9 eV, respectively. A number of p-type polymers have been blended with N2200. Ito and co-workers showed that a PTB7-Th/N2200 blend gave 5.7% PCE and 0.81 V V_{OC} , resulting in an E_{loss} of 0.64 eV.¹⁵⁵ They also reported that a blend of N2200 with p-type polymer PTQ1 (**Figure 11b**) provided a PCE of 4.1% and a V_{OC} of 0.84 V, and thus an E_{loss} of 0.61 eV.¹⁵⁶ Yang and co-workers utilized derivatives of PTQ1 in which the quinoxaline moiety was fluorinated, *i.e.*, TQ-F and TQ-FF (**Figure 11b**), in combination with N2200.¹⁵⁷ Due to the deep E_{HOMOS} for TQ-F and TQ-FF, the TQ-F/N2200 and TQ-FF/N2200 cells showed improved V_{OC} s of 0.84 and 0.94 V, respectively, relative to the PTQ1/N2200 cell that showed a V_{OC} of 0.82 V in this report. As a result, the TQ-F and TQ-FF cells had E_{loss} s of 0.61 and 0.51 eV, respectively, although the TQ-F cell showed a higher PCE of 7.3% than the TQ-FF cell of 4.14%. Wang and co-workers reported an N2200-based all-polymer cell with a BDT-quinoxaline copolymer, PBDT-DFQX1 (**Figure 11b**).¹⁵⁸ This system gave a V_{OC} of 0.89 V, and thus an E_{loss} of 0.56 eV, and a PCE of 6.7%. In addition, Huang and co-workers showed that the use of a copolymer of BDT and the imide-functionalized benzotriazole unit, PTzBI-Si (**Figure 11b**), afforded an E_{loss} of 0.59 eV.¹⁴¹ The cell demonstrated 11% PCE, which is markedly high for all-polymer cells. It is noted that although the EQE was around 70% at the absorption of PTzBI-Si, it was limited to around 50% at the absorption of N2200.

Jenekhe and co-workers synthesized a series of NDI-selenophene copolymers, BSSx (**Figure 11a**), by changing the contents of the selenophene and biselenophene co-units.¹⁵⁹ Increasing the selenophene content slightly widened E_g from 1.40 eV for BBS0 to 1.45 eV for both BBS10 and BBS20, and to 1.49 eV for BBS50. The cell that used PBDB-T as the p-type polymer showed the highest PCE of 10.1% for BBS10, among these polymers, with a V_{OC} of 0.86 V, resulting in an E_{loss}

of 0.59 eV. As similar to the PTzBI-Si/N2200 cell, although a high EQE_{max} of more than 80% was observed at around 600 nm, this should correspond to the absorption of PBDB-T, *i.e.*, the charge generation from PBDB-T to BBS10, where ΔE_{H} was a sufficiently large value of ~ 0.6 eV. On the other hand, the EQE around 700 nm, corresponding to the absorption of BBS10, was limited to 50%, although ΔE_{H} was still as large as ~ 0.5 eV.

Interestingly, n-type polymers incorporating “NFA” as the building unit were reported to show high PCEs in the all-polymer cells. Li and co-workers reported the synthesis of IDIC-based polymer PZ1 (**Figure 11a**),¹⁶⁰ which had an E_{g} of 1.55 eV and an E_{HOMO} of -5.74 eV, and thereby a ΔE_{H} of approximately 0.4 eV when PBDB-T was employed as the p-type polymer. Note that the E_{g} and the energy levels of PZ1 were shifted only slightly with respect to those of IDIC. This might originate in the fact that the π -conjugation is not fully developed along the backbone, or non-regularly polymerized IDIC units, which results in regio-isomeric components. Nevertheless, the PBDB-T/PZ1 cell showed as high as 9.2% PCE with a V_{OC} of 0.83 V, resulting in an E_{loss} of 0.72 eV. Yan and co-workers synthesized a copolymer of IDIC by incorporating a BDT moiety as the co-unit, PFBDT-IDTIC (**Figure 11a**), which provided an E_{g} of 1.62 eV and an E_{HOMO} of -5.78 eV.¹⁶¹ When PBDB-TF was employed as the p-type polymer, ΔE_{H} was approximately 0.3 eV. The PBDB-TF/PFBDT-IDTIC cell gave a V_{OC} of 0.97 V, which resulted in an E_{loss} of 0.66 eV, and a PCE of 10.3%. Zhang and co-workers reported the synthesis of a similar polymer incorporating an IDTT moiety, PN1 (**Figure 11a**).¹⁶² The E_{g} and the E_{HOMO} of PN1 were 1.55 eV and -5.71 eV, respectively, resulting in a ΔE_{H} of 0.21 eV with respect to PBDB-TF. The PBDB-TF/PN1 cell showed a V_{OC} of 1.0 V and thus an E_{loss} of 0.55 eV, and a high PCE of 10.5%. Interestingly, the EQE curve of the cell was mostly flattened at around 60%, indicating that PN1 underwent charge generation similarly to PBDB-TF despite having a significantly smaller ΔE_{H} than ΔE_{L} . Huang and co-workers reported a TPBT-based polymer PJ1 (**Figure 11a**), which had an E_{g} of 1.40 eV.¹⁶³ When PJ1 was blended with PBDB-T, the ΔE_{H} was around 0.3 eV. The cell showed a very high EQE_{max} of 80% and a high PCE of 14.4%, which was the highest value for all-polymer cells, with an E_{loss} of 0.51 eV.

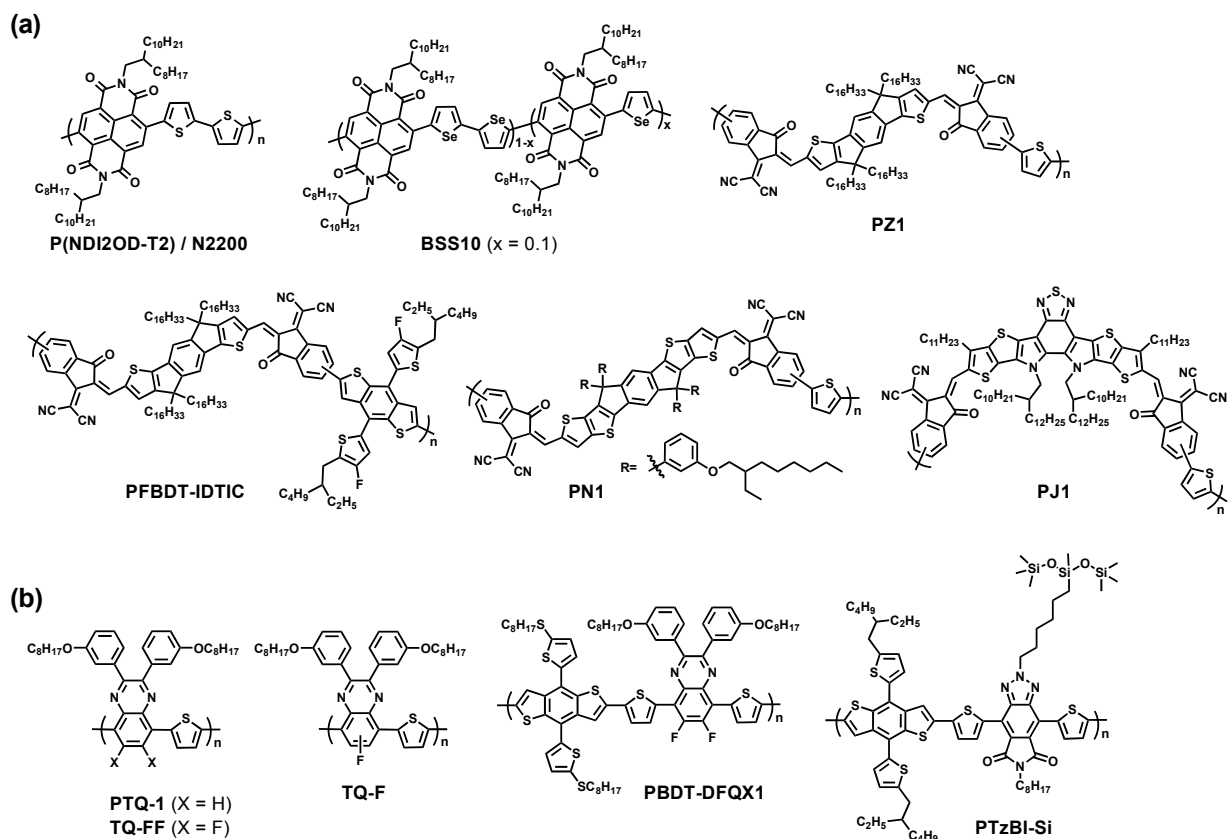


Figure 11. (a) Narrow-bandgap n-type polymers. (b) Wide-bandgap p-type polymers combined with the narrow-bandgap n-type polymers.

Table 7. Electronic and photovoltaic properties of narrow-bandgap n-type polymers

Narrow-bandgap n-type polymer	E_g (eV) ^a	$E_{\text{HOMO}}/E_{\text{LUMO}}$ (eV) ^b	p-type/ E_g (eV) ^c	ΔE_{H} (eV)	EQE_{max} (%)	J_{SC} (mA cm ⁻²)	V_{OC} (V)	FF	PCE_{max} (%)	E_{loss} (eV)	ref
P(NDI2OD-2T) (N2200)	1.45	-5.49/-4.04	PTB7-Th/ 1.58	0.70	67 ^d	12.4	0.81	0.57	5.7	0.64	155
			PTQ1/1.70	0.80	50 ^d	8.85	0.84	0.55	4.1	0.61	156
			TQ-F/ 1.76	0.55	69 ^d	13.6	0.84	0.64	7.3	0.61	157
			TQ-FF/ 1.76	0.45	46 ^d	7.57	0.94	0.58	4.1	0.51	157
			PBDT- DFQX1/ 1.77	0.03	56 ^d	11.4	0.89	0.66	6.7	0.56	158
			PTzBI-Si/ 1.78	0.50	70 ^d	16.8	0.86	0.78	11.0	0.59	141
BSS10	1.45	-5.83/-3.90	PBDB-T/ 1.82	0.48	85 ^d	18.6	0.86	0.64	10.1	0.59	159
PZ1	1.55	-5.74/-3.86	PBDB-T/ 1.82	0.41	67 ^d	16.1	0.83	0.69	9.2	0.72	160
PFBDT-IDTIC	1.62	-5.78/-3.85	PBDB-TF/ 1.80	0.24	68 ^d	15.3	0.97	0.68	10.3	0.65	161
PN1	1.55	-5.71/-3.85	PBDB-TF/ 1.80	0.21	62 ^d	15.2	1.00	0.69	10.5	0.55	162
PJ1	1.40	-5.64/-3.82	PBDT-T/ 1.82	0.26	80 ^d	22.3	0.90	0.70	14.4	0.51	163

a) Optical bandgap determined from the absorption onset. b) HOMO and LUMO energy levels determined by CV. c) p-type semiconducting polymer combined in the photovoltaic cell/optical bandgap of the polymer. d) maximum EQE value extracted from the EQE spectrum in the corresponding literature by the authors of this review.

6-3. Summary

In this section, we discussed the E_{loss} for all-polymer solar cells, in particular, by focusing on the n-type polymers, because it seemed that the reduction of E_{loss} in the all-polymer solar cells was mainly due to the development of n-type polymers. The molecular structures of the n-type polymers are relatively limited, in which imide-functionalized building units are typically incorporated. In the n-type polymers with both wide and narrow bandgaps, small E_{loss} values of less than 0.6 eV were achieved in many cases. Further, high efficiencies of more than 10% were reported in particular for all-polymer solar cells with narrow-bandgap n-type polymers based on the NDI moiety. It is noted that, however, high EQE was specifically observed in the absorption range of the p-type polymers, and the EQE at the n-type polymers was limited. This means that the charge generation from the exciton of the narrow-bandgap n-type polymers is still insufficient. One of the reasons may be that N2200 or NDI-based polymers typically have a low absorption coefficient of the order of 10^4 cm^{-1} .¹⁵⁵ Recently, narrow-bandgap n-type polymers, in which DCM-end-capped NFA were used as the building unit, have shown to afford small E_{loss} values simultaneously with high EQE_{max} and thus PCE values. This is probably due to the same reason as mentioned in the narrow-bandgap fused ring polymers and NFAs sections.

7. Summary and Outlook

We reviewed organic semiconductors and p/n blends that have resulted in small E_{loss} values for OPVs. In all the blend systems, including polymer/fullerene, polymer/non-fullerene, and polymer/polymer systems, E_{loss} was successfully reduced to below 0.6 eV, which had been considered the minimum value for OPVs, owing to the development of new π -conjugated materials that have led to a small ΔE_{H} or ΔE_{L} . In fact, an even smaller E_{loss} of around 0.5 eV, which is comparable to that for inorganic PVs, was reported for all the blend systems. This was realized by the fine tuning of frontier orbital energy levels through the design and engineering of the molecular structures of the organic semiconductors, and the optimization of the combination of p-type and n-type organic semiconductors. In fact, efficient charge generation was realized despite the fact that ΔE_{H} or ΔE_{L} was very small. Moreover, high EQE was observed even at nearly zero ΔE_{H} or ΔE_{L} , i.e., negligible driving-force energy. In particular, wide-bandgap polymer/narrow-bandgap NFA systems have higher tendency to give a small E_{loss} with a high EQE so far, yet the reason is still unclear. Apparently, a common feature in terms of molecular structure for the materials that have enabled efficient charge generation under a small E_{loss} may be the highly π -extended π -conjugated molecular structure based on large fused heteroaromatic rings and highly ordered structure in the blend film. Thus, such a molecular design might be a key factor for realizing further high performance.

On the other hand, more recently, studies on $q\Delta V_{\text{nr}}$ in OPVs have also been making progress, although reports regarding the design of π -conjugated materials for reducing the $q\Delta V_{\text{nr}}$ are still limited: $q\Delta V_{\text{nr}}$ can now be reduced even below 0.2 eV.^{22,126} One most possible explanation for such a small $q\Delta V_{\text{nr}}$ is that hybridization of LE and CT states, due to the close LE and CT states in energy, would enhance the CT emission and thus the EQE_{EL} of the OPV cells. This is partly because the PL quantum efficiency is typically high because molecular structures are relatively rigid owing to their fused-ring backbone. We should note that such a small energetic difference between LE and CT states, that is ΔE , might, however, give rise to the reduction of the charge generation efficiency and in turn the photovoltaic EQE. Thus, the LE–CT hybridization also closely relates to the minimization of ΔE .

Designing organic semiconductors by incorporating a more fluorescent chromophore and/or a rigid extended fused ring into the molecular structure might realize efficient CT emission simultaneously with efficient charge generation.

Although the E_{loss} for OPVs has been significantly reduced while showing efficient charge generation, the smallest E_{loss} values for OPVs are still larger by approximately 0.1 eV compared with those for inorganic and perovskite PVs. Additional strategy for further reducing the E_{loss} is minimizing the loss from radiative recombination ($q\Delta V_{\text{r}}$). The $q\Delta V_{\text{r}}$ values for OPVs are typically 0.2–0.6 eV, and are much larger than those for inorganic and perovskite PVs, which have the values of around 0.01 eV or even less.⁴⁷ Note that we here discuss $q\Delta V_{\text{r}}$ on the basis of E_{g} , thus ΔE is included in $q\Delta V_{\text{r}}$. As mentioned in Introduction (**Figure 2c**), $q\Delta V_{\text{r}}$ consists of two radiation losses above and below E_{g} ($q\Delta V_{\text{r1}}$ and $q\Delta V_{\text{r2}}$). In fact, the $q\Delta V_{\text{r2}}$ can be minimized, while the $q\Delta V_{\text{r1}}$ is inevitable even in the SQ limit. As the $q\Delta V_{\text{r2}}$ is partly due to the CT absorption in OPVs, it can be reduced with bringing E_{CT} closer to E_{g} , i.e., with minimizing ΔE . However, even though ΔE is negligible, the $q\Delta V_{\text{r2}}$ for OPVs still remains larger than that for inorganic and perovskite PVs,¹⁵ due to an absorption tail originating from thermal and/or structural disorder in materials, which can be quantified as Urbach energy (E_{U}). Thus, $q\Delta V_{\text{r2}}$ should be further reduced if a blend of organic semiconductors has a small E_{U} . It is noted that E_{U} values for organic semiconductors are typically more than 40 meV,¹⁶⁴ which are significantly larger than those for inorganic semiconductors that are as small as 10 meV.¹⁶⁵ As described in the Supplementary Information (Figure S3), the $q\Delta V_{\text{r2}}$ would be <0.01 eV when E_{U} is around 10 meV, being consistent with the values for inorganic and perovskite PVs, but it could be more than 0.5 eV when E_{U} is >40 meV, though depending on the E_{g} . It is thus of particular importance to suppress the E_{U} to less than the thermal energy (~25 meV) in order to reduce $q\Delta V_{\text{r2}}$: $q\Delta V_{\text{r2}}$ would be 0.06–0.07 eV when E_{U} is 25 meV. It is noted that in fact E_{U} s as close as 25 meV have been reported for some high mobility π -conjugated polymers.^{164,166} Further, some efficient OPV systems with small E_{loss} s have shown to have E_{U} values of 25–27 meV.^{22,56}

As a large number of materials have been developed so far in the area, further optimization of the combination with already available materials could yield even higher performance. Ternary blend cell, by the addition of a material with well-matched energetics with respect to the host binary blend, can also be a good strategy for reducing the E_{loss} while simultaneously increasing the photocurrent.^{167,168} Nevertheless, more in-depth exploration of π -conjugated materials based on large π -extended fused rings, specifically those having higher PL efficiency and/or less structural disorder, is warranted. On the other hand, the fundamental mechanisms of the interactions of the p-type and n-type fused ring π -conjugated materials at the interface must be studied to facilitate the charge generation under negligible driving-force energy. As the issue for the E_{loss} is directly related to the issue for the PCE improvement in OPVs, it is imperative to take up additional challenges in materials development. We hope that this review will be of help to chemists and materials scientists who are involved in the design of π -conjugated materials and blends with an eye toward highly efficient OPVs.

Acknowledgement

This study was supported by the Advanced Low Carbon Technology Research and Development Program (ALCA) of Japan Science and Technology Agency (Grant No. JPMJAL 1404), KAKENHI from Japan Society for the Promotion of Science (JSPS) (Grant Nos. 16H04196 and 19K21129), and “Next Generation Photovoltaics” Promising Research Initiatives in Hiroshima University (the Program for Enhancement of Research Universities from Ministry of Education, Culture, Sports, Science, and Technology (MEXT)).

References

1. S. Günes, H. Neugebauer and N. S. Sariciftci, *Chem. Rev.*, 2007, **107**, 1324–1338.
2. C. J. Brabec, U. Scherf, V. Dyakonov, *Organic Photovoltaics: Materials, Device Physics, and Manufacturing Technologies 2nd Ed*, Wiley-VCH, Weinheim, 2014.
3. M. Hiramoto, H. Fujiwara and M. Yokoyama, *Appl. Phys. Lett.*, 1991, **58**, 1062–1064.
4. G. Yu, J. Gao, J. C. Hummelen, F. Wudl and A. J. Heeger, *Science*, 1995, **270**, 1789.
5. J. J. M. Halls, C. A. Walsh, N. C. Greenham, E. A. Marseglia, R. H. Friend, S. C. Moratti and A. B. Holmes, *Nature*, 1995, **376**, 498–500.
6. L. Lu, T. Zheng, Q. Wu, A. M. Schneider, D. Zhao and L. Yu, *Chem. Rev.*, 2015, **115**, 12666–12731.
7. Y. He and Y. Li, *Phys. Chem. Chem. Phys.*, 2011, **13**, 1970–1983.
8. C. B. Nielsen, S. Holliday, H.-Y. Chen, S. J. Cryer and I. McCulloch, *Acc. Chem. Res.*, 2015, **48**, 2803–2812.
9. Z. Genene, W. Mammo, E. Wang and M. R. Andersson, *Adv. Mater.*, 2019, **31**, 1807275.
10. Y. Liang, Z. Xu, J. Xia, S.-T. Tsai, Y. Wu, G. Li, C. Ray and L. Yu, *Adv. Mater.*, 2010, **22**, E135–E138.
11. Z. He, C. Zhong, S. Su, M. Xu, H. Wu and Y. Cao, *Nat. Photon.*, 2012, **6**, 591.
12. I. Osaka, T. Kakara, N. Takemura, T. Koganezawa and K. Takimiya, *J. Am. Chem. Soc.*, 2013, **135**, 8834–8837.
13. Y. Liu, J. Zhao, Z. Li, C. Mu, W. Ma, H. Hu, K. Jiang, H. Lin, H. Ade and H. Yan, *Nat. Commun.*, 2014, **5**, 5293.
14. Y. Lin, J. Wang, Z.-G. Zhang, H. Bai, Y. Li, D. Zhu and X. Zhan, *Adv. Mater.*, 2015, **27**, 1170–1174.
15. J. Liu, S. Chen, D. Qian, B. Gautam, G. Yang, J. Zhao, J. Bergqvist, F. Zhang, W. Ma, H. Ade, O. Inganäs, K. Gundogdu, F. Gao and H. Yan, *Nat. Energy*, 2016, **1**, 16089.
16. W. Zhao, S. Li, H. Yao, S. Zhang, Y. Zhang, B. Yang and J. Hou, *J. Am. Chem. Soc.*, 2017, **139**, 7148–7151.
17. J. Yuan, Y. Zhang, L. Zhou, G. Zhang, H.-L. Yip, T.-K. Lau, X. Lu, C. Zhu, H. Peng, P. A. Johnson, M. Leclerc, Y. Cao, J. Ulanski, Y. Li and Y. Zou, *Joule*, 2019, **3**, 1140–1151.
18. D. Baran, R. S. Ashraf, D. A. Hanifi, M. Abdelsamie, N. Gasparini, J. A. Röhr, S. Holliday, A. Wadsworth, S. Lockett, M. Neophytou, C. J. M. Emmott, J. Nelson, C. J. Brabec, A. Amassian, A. Salleo, T. Kirchartz, J. R. Durrant and I. McCulloch, *Nat. Mater.*, 2016, **16**, 363.
19. V. Vohra, K. Kawashima, T. Kakara, T. Koganezawa, I. Osaka, K. Takimiya and H. Murata, *Nat. Photon.*, 2015, **9**, 403.

20. Q. Liu, Y. Jiang, K. Jin, J. Qin, J. Xu, W. Li, J. Xiong, J. Liu, Z. Xiao, K. Sun, S. Yang, X. Zhang and L. Ding, *Sci. Bull.*, 2020, **65**, 272–275.
21. M. A. Green, E. D. Dunlop, J. Hohl-Ebinger, M. Yoshita, N. Kopidakis and A. W. Y. Ho-Baillie, *Prog. Photovolt. Res. Appl.*, 2020, **28**, 3–15.
22. S. Liu, J. Yuan, W. Deng, M. Luo, Y. Xie, Q. Liang, Y. Zou, Z. He, H. Wu and Y. Cao, *Nat. Photon.*, 2020, **14**, 300–305.
23. Y. Cui, H. Yao, J. Zhang, K. Xian, T. Zhang, L. Hong, Y. Wang, Y. Xu, K. Ma, C. An, C. He, Z. Wei, F. Gao and J. Hou, *Adv. Mater.*, 2020, **32**, 1908205.
24. J. Zhao, A. Wang and M. A. Green, *Prog. Photovolt. Res. Appl.*, 1999, **7**, 471–474.
25. M. A. Green, *Prog. Photovolt. Res. Appl.*, 2009, **17**, 183–189.
26. Y. Liu, S. Akin, L. Pan, R. Uchida, N. Arora, J. V. Milić, A. Hinderhofer, F. Schreiber, A. R. Uhl, S. M. Zakeeruddin, A. Hagfeldt, M. I. Dar and M. Grätzel, *Sci. Adv.*, 2019, **5**, eaaw2543.
27. D. Veldman, S. C. J. Meskers and R. A. J. Janssen, *Adv. Funct. Mater.*, 2009, **19**, 1939–1948.
28. R. R. King, D. Bhusari, A. Boca, D. Larrabee, X. Q. Liu, W. Hong, C. M. Fetzer, D. C. Law and N. H. Karam, *Prog. Photovolt. Res. Appl.*, 2011, **19**, 797–812.
29. M. Wang, H. Wang, T. Yokoyama, X. Liu, Y. Huang, Y. Zhang, T.-Q. Nguyen, S. Aramaki and G. C. Bazan, *J. Am. Chem. Soc.*, 2014, **136**, 12576–12579.
30. K. Kawashima, Y. Tamai, H. Ohkita, I. Osaka and K. Takimiya, *Nat. Commun.*, 2015, **6**, 10085.
31. X. Zhou, L. Zhang, X. Wang, C. Liu, S. Chen, M. Zhang, X. Li, W. Yi and B. Xu, *Adv. Mater.*, 2020, **32**, 1908107.
32. W. Li, K. H. Hendriks, A. Furlan, M. M. Wienk and R. A. J. Janssen, *J. Am. Chem. Soc.*, 2015, **137**, 2231–2234.
33. B. C. Thompson and J. M. J. Fréchet, *Angew. Chem. Int. Ed.*, 2008, **47**, 58–77.
34. M. C. Scharber, D. Mühlbacher, M. Koppe, P. Denk, C. Waldauf, A. J. Heeger and C. J. Brabec, *Adv. Mater.*, 2006, **18**, 789–794.
35. T. M. Clarke and J. R. Durrant, *Chem. Rev.*, 2010, **110**, 6736–6767.
36. M. C. Scharber and N. S. Sariciftci, *Prog. Polym. Sci.*, 2013, **38**, 1929–1940.
37. G. Smestad, *Sol. Energy Mater. Sol. Cells*, 1993, **30**, 190.
38. W. Shockley and H. J. Queisser, *J. Appl. Phys.*, 1961, **32**, 510–519.
39. T. Kirchartz, K. Taretto and U. Rau, *J. Phys. Chem. C*, 2009, **113**, 17958–17966.
40. L. J. A. Koster, S. E. Shaheen and J. C. Hummelen, *Adv. Energy Mater.*, 2012, **2**, 1246–1253.

41. I. W. Hwang, C. Soci, D. Moses, Z. Zhu, D. Waller, R. Gaudiana, C. J. Brabec and A. J. Heeger, *Adv. Mater.*, 2007, **19**, 2307–2312.
42. H. Ohkita, S. Cook, Y. Astuti, W. Duffy, S. Tierney, W. Zhang, M. Heeney, I. McCulloch, J. Nelson, D. D. C. Bradley and J. R. Durrant, *J. Am. Chem. Soc.*, 2008, **130**, 3030–3042.
43. K. Vandewal, J. Benduhn and V. C. Nikolis, *Sustain. Energy Fuels*, 2018, **2**, 538–544.
44. S. P. McGlynn, *Chem. Rev.*, 1958, **58**, 1113–1156.
45. J. Hou, O. Inganäs, R. H. Friend and F. Gao, *Nat. Mater.*, 2018, **17**, 119.
46. J. Zhang, H. S. Tan, X. Guo, A. Facchetti and H. Yan, *Nat. Energy*, 2018, **3**, 720–731.
47. J. Yao, T. Kirchartz, M. S. Vezie, M. A. Faist, W. Gong, Z. He, H. Wu, J. Troughton, T. Watson, D. Bryant and J. Nelson, *Phys. Rev. Appl.*, 2015, **4**, 014020.
48. J. Benduhn, K. Tvingstedt, F. Piersimoni, S. Ullbrich, Y. Fan, M. Tropicano, K. A. McGarry, O. Zeika, M. K. Riede, C. J. Douglas, S. Barlow, S. R. Marder, D. Neher, D. Spoltore and K. Vandewal, *Nat. Energy*, 2017, **2**, 17053.
49. D. Qian, Z. Zheng, H. Yao, W. Tress, T. R. Hopper, S. Chen, S. Li, J. Liu, S. Chen, J. Zhang, X.-K. Liu, B. Gao, L. Ouyang, Y. Jin, G. Pozina, I. A. Buyanova, W. M. Chen, O. Inganäs, V. Coropceanu, J.-L. Bredas, H. Yan, J. Hou, F. Zhang, A. A. Bakulin and F. Gao, *Nat. Mater.*, 2018, **17**, 703–709.
50. X.-K. Chen, V. Coropceanu and J.-L. Brédas, *Nat. Commun.*, 2018, **9**, 5295.
51. F. D. Eisner, M. Azzouzi, Z. Fei, X. Hou, T. D. Anthopoulos, T. J. S. Dennis, M. Heeney and J. Nelson, *J. Am. Chem. Soc.*, 2019, **141**, 6362–6374.
52. T. Saito, S.-i. Natsuda, K. Imakita, Y. Tamai and H. Ohkita, *Solar RRL*, 2020, **4**, 2000255.
53. U. Rau, *Phys. Rev. B*, 2007, **76**, 085303.
54. K. Vandewal, K. Tvingstedt, A. Gadisa, O. Inganäs and J. V. Manca, *Phys. Rev. B*, 2010, **81**, 125204.
55. Y. Wang, D. Qian, Y. Cui, H. Zhang, J. Hou, K. Vandewal, T. Kirchartz and F. Gao, *Adv. Energy Mater.*, 2018, **8**, 1801352.
56. N. A. Ran, J. A. Love, C. J. Takacs, A. Sadhanala, J. K. Beavers, S. D. Collins, Y. Huang, M. Wang, R. H. Friend, G. C. Bazan and T.-Q. Nguyen, *Adv. Mater.*, 2016, **28**, 1482–1488.
57. J. Gierschner, J. Cornil and H. J. Egelhaaf, *Adv. Mater.*, 2007, **19**, 173–191.
58. V. C. Nikolis, J. Benduhn, F. Holzmueller, F. Piersimoni, M. Lau, O. Zeika, D. Neher, C. Koerner, D. Spoltore and K. Vandewal, *Adv. Energy Mater.*, 2017, **7**, 1700855.
59. H. Yoshida, *Chem. Phys. Lett.*, 2012, **539–540**, 180–185.
60. H. Yoshida, *J. Electron Spectrosc. Relat. Phenom.*, 2015, **204**, 116–124.
61. J.-L. Brédas, J. E. Norton, J. Cornil and V. Coropceanu, *Acc. Chem. Res.*, 2009, **42**, 1691–1699.

62. J. C. Hummelen, B. W. Knight, F. LePeq, F. Wudl, J. Yao and C. L. Wilkins, *J. Org. Chem.*, 1995, **60**, 532–538.
63. M. M. Wienk, J. M. Kroon, W. J. H. Verhees, J. Knol, J. C. Hummelen, P. A. van Hal and R. A. J. Janssen, *Angew. Chem. Int. Ed.*, 2003, **42**, 3371–3375.
64. M. Lenes, G.-J. A. H. Wetzelaer, F. B. Kooistra, S. C. Veenstra, J. C. Hummelen and P. W. M. Blom, *Adv. Mater.*, 2008, **20**, 2116–2119.
65. Y. He, H.-Y. Chen, J. Hou and Y. Li, *J. Am. Chem. Soc.*, 2010, **132**, 1377–1382.
66. G. Li, V. Shrotriya, J. Huang, Y. Yao, T. Moriarty, K. Emery and Y. Yang, *Nat. Mater.*, 2005, **4**, 864–868.
67. H. Xu, H. Ohkita, Y. Tamai, H. Benten and S. Ito, *Adv. Mater.*, 2015, **27**, 5868–5874.
68. Y. Li, *Chem. Asian J.*, 2013, **8**, 2316–2328.
69. A. Mohajeri and A. Omidvar, *Phys. Chem. Chem. Phys.*, 2015, **17**, 22367–22376.
70. R. Ganesamoorthy, G. Sathiyam and P. Sakthivel, *Sol. Energy Mater. Sol. Cells*, 2017, **161**, 102–148.
71. F. Padinger, C. Brabec, T. Fromherz, J. C. Hummelen and N. S. Sariciftci, *Opto-electron. Rev.*, 2000, **8**, 280–283.
72. D. Gebeyehu, C. J. Brabec, F. Padinger, T. Fromherz, J. C. Hummelen, D. Badt, H. Schindler and N. S. Sariciftci, *Synth. Met.*, 2001, **118**, 1–9.
73. F. Padinger, T. Fromherz, J. C. Hummelen and N. S. Sariciftci, *Bull. Chem. Soc. Ethiop.*, 2000, **14**, 57.
74. D. Gebeyehu, F. Padinger, C. J. Brabec, T. Fromherz, J. C. Hummelen and N. S. Sariciftci, *Int. J. Photoenergy*, 1999, **1**, 95.
75. T. Fromherz, F. Padinger, D. Gebeyehu, C. Brabec, J. C. Hummelen and N. S. Sariciftci, *Sol. Energy Mater. Sol. Cells*, 2000, **63**, 61–68.
76. *US Pat.*, WO 2008/018931A2, 2008.
77. Y. Matsuo, Y. Sato, T. Niinomi, I. Soga, H. Tanaka and E. Nakamura, *J. Am. Chem. Soc.*, 2009, **131**, 16048–16050.
78. Y. Matsuo, A. Ozu, N. Obata, N. Fukuda, H. Tanaka and E. Nakamura, *Chem. Commun.*, 2012, **48**, 3878–3880.
79. S. Zhang, L. Ye, W. Zhao, D. Liu, H. Yao and J. Hou, *Macromolecules*, 2014, **47**, 4653–4659.
80. Q. Wan, X. Guo, Z. Wang, W. Li, B. Guo, W. Ma, M. Zhang and Y. Li, *Adv. Funct. Mater.*, 2016, **26**, 6635–6640.
81. M. Kim, W.-T. Park, S. A. Park, C. W. Park, S. U. Ryu, D. H. Lee, Y.-Y. Noh and T. Park, *Adv. Funct. Mater.*, 2019, **29**, 1805994.

82. L. Yang, J. R. Tumbleston, H. Zhou, H. Ade and W. You, *Energy Environ. Sci.*, 2013, **6**, 316–326.
83. A. C. Stuart, J. R. Tumbleston, H. Zhou, W. Li, S. Liu, H. Ade and W. You, *J. Am. Chem. Soc.*, 2013, **135**, 1806–1815.
84. S. C. Price, A. C. Stuart, L. Yang, H. Zhou and W. You, *J. Am. Chem. Soc.*, 2011, **133**, 4625–4631.
85. I. Osaka, M. Shimawaki, H. Mori, I. Doi, E. Miyazaki, T. Koganezawa and K. Takimiya, *J. Am. Chem. Soc.*, 2012, **134**, 3498–3507.
86. K. Kawashima, T. Fukuhara, Y. Suda, Y. Suzuki, T. Koganezawa, H. Yoshida, H. Ohkita, I. Osaka and K. Takimiya, *J. Am. Chem. Soc.*, 2016, **138**, 10265–10275.
87. M. Saito, T. Fukuhara, S. Kamimura, H. Ichikawa, H. Yoshida, T. Koganezawa, Y. Ie, Y. Tamai, H. D. Kim, H. Ohkita and I. Osaka, *Adv. Energy Mater.*, 2020, **10**, 1903278.
88. Z. Du, X. Bao, Y. Li, D. Liu, J. Wang, C. Yang, R. Wimmer, L. W. Städe, R. Yang and D. Yu, *Adv. Energy Mater.*, 2017, **8**, 1701471.
89. K. Kawashima, I. Osaka and K. Takimiya, *Chem. Mater.*, 2015, **27**, 6558–6570.
90. Z. Zhang, F. Lin, H.-C. Chen, H.-C. Wu, C.-L. Chung, C. Lu, S.-H. Liu, S.-H. Tung, W.-C. Chen, K.-T. Wong and P.-T. Chou, *Energy Environ. Sci.*, 2015, **8**, 552–557.
91. L. Bianchi, X. Zhang, Z. Chen, P. Chen, X. Zhou, Y. Tang, B. Liu, X. Guo and A. Facchetti, *Chem. Mater.*, 2019, **31**, 6519–6529.
92. C. Dyer-Smith, L. X. Reynolds, A. Bruno, D. D. C. Bradley, S. A. Haque and J. Nelson, *Adv. Funct. Mater.*, 2010, **20**, 2701–2708.
93. C. W. Schlenker, K.-S. Chen, H.-L. Yip, C.-Z. Li, L. R. Bradshaw, S. T. Ochsenbein, F. Ding, X. S. Li, D. R. Gamelin, A. K. Y. Jen and D. S. Ginger, *J. Am. Chem. Soc.*, 2012, **134**, 19661–19668.
94. A. Wadsworth, M. Moser, A. Marks, M. S. Little, N. Gasparini, C. J. Brabec, D. Baran and I. McCulloch, *Chem. Soc. Rev.*, 2019, **48**, 1596–1625
95. G. Zhang, J. Zhao, P. C. Y. Chow, K. Jiang, J. Zhang, Z. Zhu, J. Zhang, F. Huang and H. Yan, *Chem. Rev.*, 2018, **118**, 3447–3507.
96. J. J. Dittmer, K. Petritsch, E. A. Marseglia, R. H. Friend, H. Rost and A. B. Holmes, *Synth. Met.*, 1999, **102**, 879–880.
97. L. Schmidt-Mende, A. Fechtenkötter, K. Müllen, E. Moons, R. H. Friend and J. D. MacKenzie, *Science*, 2001, **293**, 1119.
98. R. Singh, E. Aluicio-Sarduy, Z. Kan, T. Ye, R. C. I. MacKenzie and P. E. Keivanidis, *J. Mater. Chem. A*, 2014, **2**, 14348–14353.
99. J. Zhao, Y. Li, H. Lin, Y. Liu, K. Jiang, C. Mu, T. Ma, J. Y. Lin Lai, H. Hu, D. Yu and H. Yan, *Energy Environ. Sci.*, 2015, **8**, 520–525.

100. J. Lee, R. Singh, D. H. Sin, H. G. Kim, K. C. Song and K. Cho, *Adv. Mater.*, 2016, **28**, 69–76.
101. Y. Liu, J. Y. L. Lai, S. Chen, Y. Li, K. Jiang, J. Zhao, Z. Li, H. Hu, T. Ma, H. Lin, J. Liu, J. Zhang, F. Huang, D. Yu and H. Yan, *J. Mater. Chem. A*, 2015, **3**, 13632–13636.
102. S.-Y. Liu, C.-H. Wu, C.-Z. Li, S.-Q. Liu, K.-H. Wei, H.-Z. Chen and A. K. Y. Jen, *Adv. Sci.*, 2015, **2**, 1500014.
103. H. Lin, S. Chen, H. Hu, L. Zhang, T. Ma, J. Y. L. Lai, Z. Li, A. Qin, X. Huang, B. Tang and H. Yan, *Adv. Mater.*, 2016, **28**, 8546–8551.
104. Y. Liu, C. Mu, K. Jiang, J. Zhao, Y. Li, L. Zhang, Z. Li, J. Y. L. Lai, H. Hu, T. Ma, R. Hu, D. Yu, X. Huang, B. Z. Tang and H. Yan, *Adv. Mater.*, 2015, **27**, 1015–1020.
105. J. Zhang, Y. Li, J. Huang, H. Hu, G. Zhang, T. Ma, P. C. Y. Chow, H. Ade, D. Pan and H. Yan, *J. Am. Chem. Soc.*, 2017, **139**, 16092–16095.
106. D. Baran, T. Kirchartz, S. Wheeler, S. Dimitrov, M. Abdelsamie, J. Gorman, R. S. Ashraf, S. Holliday, A. Wadsworth, N. Gasparini, P. Kaienburg, H. Yan, A. Amassian, C. J. Brabec, J. R. Durrant and I. McCulloch, *Energy Environ. Sci.*, 2016, **9**, 3783–3793.
107. S. Chen, Y. Wang, L. Zhang, J. Zhao, Y. Chen, D. Zhu, H. Yao, G. Zhang, W. Ma, R. H. Friend, P. C. Y. Chow, F. Gao and H. Yan, *Adv. Mater.*, 2018, **30**, 1804215.
108. W. Zhao, D. Qian, S. Zhang, S. Li, O. Inganäs, F. Gao and J. Hou, *Adv. Mater.*, 2016, **28**, 4734–4739.
109. H. Zhang, H. Yao, J. Hou, J. Zhu, J. Zhang, W. Li, R. Yu, B. Gao, S. Zhang and J. Hou, *Adv. Mater.*, 2018, **30**, 1800613.
110. S. Li, L. Ye, W. Zhao, S. Zhang, S. Mukherjee, H. Ade and J. Hou, *Adv. Mater.*, 2016, **28**, 9423–9429.
111. S. Li, L. Zhan, C. Sun, H. Zhu, G. Zhou, W. Yang, M. Shi, C.-Z. Li, J. Hou, Y. Li and H. Chen, *J. Am. Chem. Soc.*, 2019, **141**, 3073–3082.
112. H. Yao, Y. Chen, Y. Qin, R. Yu, Y. Cui, B. Yang, S. Li, K. Zhang and J. Hou, *Adv. Mater.*, 2016, **28**, 8283–8287.
113. H. Yao, Y. Cui, R. Yu, B. Gao, H. Zhang and J. Hou, *Angew. Chem. Int. Ed.*, 2017, **56**, 3045–3049.
114. Y. Cui, C. Yang, H. Yao, J. Zhu, Y. Wang, G. Jia, F. Gao and J. Hou, *Adv. Mater.*, 2017, **29**, 1703080.
115. X. Liao, Z. Yao, K. Gao, X. Shi, L. Zuo, Z. Zhu, L. Chen, F. Liu, Y. Chen and A. K. Y. Jen, *Adv. Energy Mater.*, 2018, **8**, 1801214.
116. H.-H. Gao, Y. Sun, X. Wan, X. Ke, H. Feng, B. Kan, Y. Wang, Y. Zhang, C. Li and Y. Chen, *Adv. Sci.*, 2018, **5**, 1800307.
117. H. Li, Z. Xiao, L. Ding and J. Wang, *Sci. Bull.*, 2018, **63**, 340–342.
118. Z. Xiao, X. Jia and L. Ding, *Sci. Bull.*, 2017, **62**, 1562–1564.

119. Q. Zhao, Z. Xiao, J. Qu, L. Liu, H. Richter, W. Chen, L. Han, M. Wang, J. Zheng, Z. Xie, L. Ding and F. He, *ACS Energy Lett.*, 2019, **4**, 1106–1114.
120. Z. Xiao, S. Yang, Z. Yang, J. Yang, H.-L. Yip, F. Zhang, F. He, T. Wang, J. Wang, Y. Yuan, H. Yang, M. Wang and L. Ding, *Adv. Mater.*, 2019, **31**, 1804790.
121. Z. Xiao, X. Jia, D. Li, S. Wang, X. Geng, F. Liu, J. Chen, S. Yang, T. P. Russell and L. Ding, *Sci. Bull.*, 2017, **62**, 1494–1496.
122. Z. Yao, X. Liao, K. Gao, F. Lin, X. Xu, X. Shi, L. Zuo, F. Liu, Y. Chen and A. K. Y. Jen, *J. Am. Chem. Soc.*, 2018, **140**, 2054–2057.
123. J. Yuan, Y. Zhang, L. Zhou, C. Zhang, T.-K. Lau, G. Zhang, X. Lu, H.-L. Yip, S. K. So, S. Beaupré, M. Mainville, P. A. Johnson, M. Leclerc, H. Chen, H. Peng, Y. Li and Y. Zou, *Adv. Mater.*, 2019, **31**, 1807577.
124. Y. Cui, H. Yao, J. Zhang, T. Zhang, Y. Wang, L. Hong, K. Xian, B. Xu, S. Zhang, J. Peng, Z. Wei, F. Gao and J. Hou, *Nat. Commun.*, 2019, **10**, 2515.
125. C. Yao, B. Liu, Y. Zhu, L. Hong, J. Miao, J. Hou, F. He and H. Meng, *J. Mater. Chem. A*, 2019, **7**, 10212–10216.
126. Y. Xu, H. Yao, L. Ma, L. Hong, J. Li, Q. Liao, Y. Zu, J. Wang, M. Gao, L. Ye and J. Hou, *Angew. Chem. Int. Ed.*, 2020, **59**, 9004–9010.
127. D. Qian, L. Ye, M. Zhang, Y. Liang, L. Li, Y. Huang, X. Guo, S. Zhang, Z. Tan and J. Hou, *Macromolecules*, 2012, **45**, 9611–9617.
128. T. J. Aldrich, S. M. Swick, F. S. Melkonyan and T. J. Marks, *Chem. Mater.*, 2017, **29**, 10294–10298.
129. Q. Fan, Y. Wang, M. Zhang, B. Wu, X. Guo, Y. Jiang, W. Li, B. Guo, C. Ye, W. Su, J. Fang, X. Ou, F. Liu, Z. Wei, T. C. Sum, T. P. Russell and Y. Li, *Adv. Mater.*, 2017, **30**, 1704546.
130. S. Zhang, Y. Qin, J. Zhu and J. Hou, *Adv. Mater.*, 2018, **30**, 1800868.
131. X. Xu, T. Yu, Z. Bi, W. Ma, Y. Li and Q. Peng, *Adv. Mater.*, 2017, **30**, 1703973.
132. X. Xu, Z. Li, Z. Bi, T. Yu, W. Ma, K. Feng, Y. Li and Q. Peng, *Adv. Mater.*, 2018, **30**, 1800737.
133. J. Liu, L. Liu, C. Zuo, Z. Xiao, Y. Zou, Z. Jin and L. Ding, *Sci. Bull.*, 2019, **64**, 1655–1657.
134. J. Xiong, K. Jin, Y. Jiang, J. Qin, T. Wang, J. Liu, Q. Liu, H. Peng, X. Li, A. Sun, X. Meng, L. Zhang, L. Liu, W. Li, Z. Fang, X. Jia, Z. Xiao, Y. Feng, X. Zhang, K. Sun, S. Yang, S. Shi and L. Ding, *Sci. Bull.*, 2019, **64**, 1573–1576.
135. C. Sun, F. Pan, H. Bin, J. Zhang, L. Xue, B. Qiu, Z. Wei, Z.-G. Zhang and Y. Li, *Nat. Commun.*, 2018, **9**, 743.
136. C. Sun, S. Qin, R. Wang, S. Chen, F. Pan, B. Qiu, Z. Shang, L. Meng, C. Zhang, M. Xiao, C. Yang and Y. Li, *J. Am. Chem. Soc.*, 2020, **142**, 1465–1474.

137. S. Chen, Y. Liu, L. Zhang, P. C. Y. Chow, Z. Wang, G. Zhang, W. Ma and H. Yan, *J. Am. Chem. Soc.*, 2017, **139**, 6298–6301.
138. J. Wang, J. Xu, N. Yao, D. Zhang, Z. Zheng, S. Xie, X. Zhang, F. Zhang, H. Zhou, C. Zhang and Y. Zhang, *J. Phys. Chem. Lett.*, 2019, **10**, 4110–4116.
139. G. Wang, F. S. Melkonyan, A. Facchetti and T. J. Marks, *Angew. Chem. Int. Ed.*, 2019, **58**, 4129–4142.
140. C. Lee, S. Lee, G.-U. Kim, W. Lee and B. J. Kim, *Chem. Rev.*, 2019, **119**, 8028–8086.
141. Z. Li, L. Ying, P. Zhu, W. Zhong, N. Li, F. Liu, F. Huang and Y. Cao, *Energy Environ. Sci.*, 2019, **12**, 157–163.
142. E. Zhou, J. Cong, Q. Wei, K. Tajima, C. Yang and K. Hashimoto, *Angew. Chem. Int. Ed.*, 2011, **50**, 2799–2803.
143. Y. Zhou, T. Kurosawa, W. Ma, Y. Guo, L. Fang, K. Vandewal, Y. Diao, C. Wang, Q. Yan, J. Reinspach, J. Mei, A. L. Appleton, G. I. Koleilat, Y. Gao, S. C. B. Mannsfeld, A. Salleo, H. Ade, D. Zhao and Z. Bao, *Adv. Mater.*, 2014, **26**, 3767–3772.
144. S. Liu, Z. Kan, S. Thomas, F. Cruciani, J.-L. Brédas and P. M. Beaujuge, *Angew. Chem. Int. Ed.*, 2016, **55**, 12996–13000.
145. X. Guo, A. Facchetti and T. J. Marks, *Chem. Rev.*, 2014, **114**, 8943–9021.
146. X. Guo, R. P. Ortiz, Y. Zheng, Y. Hu, Y.-Y. Noh, K.-J. Baeg, A. Facchetti and T. J. Marks, *J. Am. Chem. Soc.*, 2011, **133**, 1405–1418.
147. X. Guo, N. Zhou, S. J. Lou, J. W. Hennek, R. Ponce Ortiz, M. R. Butler, P.-L. T. Boudreault, J. Strzalka, P.-O. Morin, M. Leclerc, J. T. López Navarrete, M. A. Ratner, L. X. Chen, R. P. H. Chang, A. Facchetti and T. J. Marks, *J. Am. Chem. Soc.*, 2012, **134**, 18427–18439.
148. M. Saito, I. Osaka, Y. Suda, H. Yoshida and K. Takimiya, *Adv. Mater.*, 2016, **28**, 6921–6925.
149. H. Sun, Y. Tang, C. W. Koh, S. Ling, R. Wang, K. Yang, J. Yu, Y. Shi, Y. Wang, H. Y. Woo and X. Guo, *Adv. Mater.*, 2019, **31**, 1807220.
150. Y. Wang, Z. Yan, H. Guo, M. A. Uddin, S. Ling, X. Zhou, H. Su, J. Dai, H. Y. Woo and X. Guo, *Angew. Chem. Int. Ed.*, 2017, **56**, 15304–15308.
151. H. Sun, B. Liu, C. W. Koh, Y. Zhang, J. Chen, Y. Wang, P. Chen, B. Tu, M. Su, H. Wang, Y. Tang, Y. Shi, H. Y. Woo and X. Guo, *Adv. Funct. Mater.*, 2019, **29**, 1903970.
152. X. Long, Z. Ding, C. Dou, J. Zhang, J. Liu and L. Wang, *Adv. Mater.*, 2016, **28**, 6504–6508.
153. H. Yan, Z. Chen, Y. Zheng, C. Newman, J. R. Quinn, F. Dötz, M. Kastler and A. Facchetti, *Nature*, 2009, **457**, 679–686.
154. S. Fabiano, Z. Chen, S. Vahedi, A. Facchetti, B. Pignataro and M. A. Loi, *J. Mater. Chem.*, 2011, **21**, 5891–5896.

155. H. Benten, T. Nishida, D. Mori, H. Xu, H. Ohkita and S. Ito, *Energy Environ. Sci.*, 2016, **9**, 135–140.
156. D. Mori, H. Benten, I. Okada, H. Ohkita and S. Ito, *Adv. Energy Mater.*, 2014, **4**, 1301006.
157. S. Chen, Y. An, G. K. Dutta, Y. Kim, Z.-G. Zhang, Y. Li and C. Yang, *Adv. Funct. Mater.*, 2017, **27**, 1603564.
158. X. Chen, M. Zhao, Z.-g. Zhang, Y. Li, X. Li and H. Wang, *ACS Appl. Energy Mater.*, 2018, **1**, 2350–2357.
159. N. B. Kolhe, D. K. Tran, H. Lee, D. Kuzuhara, N. Yoshimoto, T. Koganezawa and S. A. Jenekhe, *ACS Energy Lett.*, 2019, **4**, 1162–1170.
160. Z.-G. Zhang, Y. Yang, J. Yao, L. Xue, S. Chen, X. Li, W. Morrison, C. Yang and Y. Li, *Angew. Chem. Int. Ed.*, 2017, **56**, 13503–13507.
161. H. Yao, F. Bai, H. Hu, L. Arunagiri, J. Zhang, Y. Chen, H. Yu, S. Chen, T. Liu, J. Y. L. Lai, Y. Zou, H. Ade and H. Yan, *ACS Energy Lett.*, 2019, **4**, 417–422.
162. J. Wu, Y. Meng, X. Guo, L. Zhu, F. Liu and M. Zhang, *J. Mater. Chem. A*, 2019, **7**, 16190–16196.
163. T. Jia, J. Zhang, W. Zhong, Y. Liang, K. Zhang, S. Dong, L. Ying, F. Liu, X. Wang, F. Huang and Y. Cao, *Nano Energy*, 2020, **72**, 104718.
164. D. Venkateshvaran, M. Nikolka, A. Sadhanala, V. Lemaire, M. Zelazny, M. Kepa, M. Hurhangee, A. J. Kronemeijer, V. Pecunia, I. Nasrallah, I. Romanov, K. Broch, I. McCulloch, D. Emin, Y. Olivier, J. Cornil, D. Beljonne and H. Sirringhaus, *Nature*, 2014, **515**, 384–388.
165. J. Jean, T. S. Mahony, D. Bozyigit, M. Sponseller, J. Holovský, M. G. Bawendi and V. Bulović, *ACS Energy Lett.*, 2017, **2**, 2616–2624.
166. A. Wadsworth, H. Chen, K. J. Thorley, C. Cendra, M. Nikolka, H. Bristow, M. Moser, A. Salleo, T. D. Anthopoulos, H. Sirringhaus and I. McCulloch, *J. Am. Chem. Soc.*, 2020, **142**, 652–664.
167. X. Ma, Q. An, O. A. Ibraikulov, P. Lévêque, T. Heiser, N. Leclerc, X. Zhang and F. Zhang, *J. Mater. Chem. A*, 2020, **8**, 1265–1272.
168. X. Ma, J. Wang, J. Gao, Z. Hu, C. Xu, X. Zhang and F. Zhang, *Adv. Energy Mater.*, 2020, **10**, 2001404.